Inaugural – Dissertation

---

zur Erlangung der Doktorwürde der
Naturwissenschaftlich-Mathematischen Gesamtfakultät
der Ruprecht-Karls-Universität in Heidelberg

vorgelegt von Diplom-Mineraloge Thorsten Agemar aus Wasserlos

Temporal Variations of δ^2H, $\delta^{18}O$ and Deuterium Excess in Atmospheric Moisture and Improvements in the CO_2-H_2O Equilibration Technique for $^{18}O/^{16}O$ Isotope Ratio Analysis

Gutachter: Prof. Dr. rer. nat. Augusto Mangini
Prof. Dr. rer. nat. Ulrich Platt

Dissertation

submitted to the

Combined Faculties for the Natural Sciences and for Mathematics

of the Ruperto-Carola University of Heidelberg, Germany

for the Doctor of Natural Sciences

presented by

Dipl.-Min. Thorsten Agemar
born in: Wasserlos, Germany

Temporal Variations of δ^2H, $\delta^{18}O$ and Deuterium Excess in Atmospheric Moisture and Improvements in the CO_2-H_2O Equilibration Technique for $^{18}O/^{16}O$ Isotope Ratio Analysis

Referees: Prof. Dr. rer. nat. Augusto Mangini
Prof. Dr. rer. nat. Ulrich Platt

Acknowledgements

For supervision of my work and for helpful discussions I would like to thank Dr. Andreas Zahn. I really appreciated his encouragement and motivating ideas.
I am very grateful to Mrs. Christel Facklam for the excellent co-operation in the stable isotope lab. Without her great support the progress made in $\delta^{18}O$ measurements would not have been possible.
I wish to express my gratitude to Prof. Dr. Ulrich Platt for the excellent working conditions and his overall guidance during this doctoral research.
I thank Prof. Dr. Kasimierz Rozanski and Prof. Dr. Christian Sonntag for careful reviews of my manuscript and helpful discussions. My special thanks go to Dr. Thomas Wagner and Stefan Höppner for being very good friends and for proof-reading my manuscript.
Last but not least, I am very grateful to my family, Ilka and Nick, for their patience and support.

Contents

1

Introduction

The stable isotope ratios of oxygen ($^{18}O/^{16}O$) and hydrogen ($^{2}H/^{1}H$) in water vapour and precipitation have become an important issue in the field of climate variability and prediction. In order to retrieve climatic information from isotope records preserved in geologic archives such as polar ice sheets, ground water, lake sediments, or fluid inclusions trapped in growing cave deposits, the processes controlling the stable isotope composition of water vapour and meteoric precipitation must be known.

The application of stable isotopes in the analysis of past and future climate changes generally involves empirical estimates of the modern spatial relationship between the isotopic composition of precipitation and ground temperature. Global scale variations in the stable isotopic composition of modern meteoric waters are well-documented (Dansgaard 1964; Rozanski et al. 1993).

The first reports of the isotopic composition of fresh waters world-wide were published by Dansgaard (1954) and Craig (1961). Also in 1961, the International Atomic Energy Agency (IAEA) in co-operation with the World Meteorological Organization (WMO) started a world-wide survey of the isotope composition of monthly precipitation (IAEA/WMO 1999). This programme was later named the Global Network of Isotopes in Precipitation (GNIP). It provides a comprehensive dataset on the isotope content (^{18}O, deuterium and tritium) of precipitation and meteorological parameters (amount and type of precipitation, air temperature and vapour pressure) on a global scale. The number of stations involved in this network varied mostly between 80 and 100 and reached a maximum of about 220 stations in 1963-64. After just three years of operation, Dansgaard (1964) gave his renowned evaluation of the record, explaining the observed relationships between heavy isotope content, amount of precipitation, air temperature, and geographical parameters characterizing the given sampling site, such as altitude, latitude, and distance from the coast. He showed that the isotopic composition of precipitation at mid and high latitudes corresponds to a Rayleigh-type condensation process of atmospheric water vapour.

In the following years, the GNIP dataset has repeatedly been statistically analysed. A growing number of reviews essentially confirms the early findings of Dansgaard (Rozanski 1993 *et al.* and references therein).

The analysis of present-day co-variations between stable isotopes in precipitation and climate-related parameters is an important step in the interpretation of isotope records in geologic archives. Unfortunately, only 32 stations world-wide have at least 20 years of ^{18}O data available (Rozanski *et al.* 1993). The calibration of such a 'paleo-isotope-thermometer' is also hampered by such effects as a changing vegetation cover, varying sea ice extent or modification of seasonal snow accumulation or ground water recharge. Recently, borehole thermometry in central Greenland revealed much cooler surface temperatures during the Last Glacial Maximum (LGM) than inferred from the isotopic composition of the ice and the modern spatial $\delta^{18}O$–T relationship (Cuffey *et al.* 1995). One possible explanation for the discrepancy could be cooler sea surface temperatures in the water vapour source region during the LGM (Boyle 1997). Several other explanations have been offered as well (Jouzel *et al.* 1997 and references therein).

A more accurate calibration of a paleo-isotope-thermometer may be achieved by General Circulation Models (GCMs) or other complex models which include a highly parameterized hydrological cycle linked to changing feedback mechanisms between atmosphere, biosphere and hydrosphere. GCMs have been repeatedly employed to simulate global scale variations in the stable isotopic compositions of precipitation (Armengaud *et al.* 1998, Hoffmann *et al.* 1999, Jouzel & Koster 1996). A recent investigation of the two most advanced GCMs (ECHAM and GISS) by Hoffman *et al.* (2000) reproduced seasonal and annual variations of stable isotopes in precipitation in good agreement with regional observations. But GCM simulations of the last glacial maximum (21 kyr BP) still have problems with important aspects of the hydrological cycle such as sea surface temperature, strength of the temperature inversion over Greenland or the seasonality of precipitation events.

In this context, it has to be discussed, to what extend the isotope precipitation data can be used as tracer for the atmospheric water vapour circulation. It has been shown that the isotope content of monthly composite precipitation samples is not necessarily in isotopic equilibrium with the monthly composites of atmospheric moisture (Schoch-Fischer et al. 1984). Topographic details are usually smoothed out by the low horizontal resolution of GCMs although they are important for the isotopic composition of precipitation. Furthermore, precipitation is available only in a more or less sporadic manner. The choice of the sampling site is crucial because spatial variations of amount and isotopic composition of precipitation affect observed values.

An alternative is the collection of water vapour which can be performed continuously, as it has been done at the Institut für Umweltphysik at Heidelberg (IUP) for more than 18 years. Previous analyses of the water vapour record (Sonntag &

Schoch-Fischer 1984, Jacob 1992, Jacob & Sonntag 1991 and references therein) demonstrated the high quality of the record and the usefulness of atmospheric water vapour as tracer for atmospheric processes.

Long-term records of the isotopic composition of water vapour are an excellent tool to investigate the response of the isotopic composition of precipitation and water vapour to long-term fluctuations of key climatic parameters (e.g. air temperature, relative humidity etc.).

The key aim of this study is a comprehensive characterisation of present day stable isotope compositions in water vapour and precipitation. The combination of data from the 18-year record of stable isotopes in atmospheric water vapour at Heidelberg, the GNIP project, and air mass back trajectories provides the basis for a qualitative interpretation of stable isotopes in the atmospheric branch of the hydrologic cycle. The given data are also used for a re-assessment of the deuterium excess, a parameter commonly used to derive information on distant vapour source regions.

Furthermore, qualitative results are simulated in a 1-D advection model using back trajectories, precipitation data, and gridded meteorologic data as input parameters.

The progress of the CO_2-H_2O equilibration method of $\delta^{18}O$ is also discussed in full detail. A system designed for high throughput has been optimized to yield results of excellent precision. Results of an 18 months study of three laboratory standard waters and an international interlaboratory comparison organized by the IAEA shows the high analytical precision of $\delta^{18}O$ determinations in natural waters now available.

2

Definitions

Oxygen has three stable isotopes whose abundances on earth are ^{16}O = 99.7621%, ^{17}O = 0.0379%, and ^{18}O = 0.2000% in V-SMOW (Vienna Standard Mean Ocean Water). Hydrogen has two stable isotopes whose abundance are 99.984% (^{1}H) and 0.0156% (^{2}H) in V-SMOW. V-SMOW is the standard reference for oxygen and hydrogen isotopes and is distributed by the International Atomic Energy Agency in Vienna (IAEA). It has the same isotopic composition as the original SMOW which was defined by H. Craig (1961) with reference to a large volume of distilled water distributed by the National Bureau of Standards in the United States (NBS-1).

In principle, geochemical and environmental investigations do not rely on the absolute isotopic ratios of standards and other materials. Isotopic analyses are commonly presented as differences of $^{18}O/^{16}O$ and $^{2}H/^{1}H$ (= D/H) ratios relative to V-SMOW on a per mil scale:

$$\delta = \left(\frac{R_{sample}}{R_{V-SMOW}} - 1\right) \cdot 1000‰ \tag{2.1}$$

where R is the isotope concentration ratio (e.g. $^{18}O/^{16}O$ or D/H). Positive δ-values indicate enrichment of a sample in the rare isotope compared to V-SMOW, whereas negative values imply depletion of those isotopes in the sample. The IAEA also distributes a second standard called SLAP (Standard Light Antarctic Precipitation) which has a $\delta^{18}O$ value of –55.50‰ and a δD value of –428.0‰. These two reference materials cover a wide range of isotopic compositions in terrestrial samples and allow a precise calibration and correction for instrumental factors in the laboratory.

A third standard, based on CO_2 produced by the reaction of 100% phosphoric acid at 25°C with Cretaceous belemnites of the PeeDee Formation in South Carolina (known as PDB), is also used to express the oxygen and carbon isotope composition in carbonates and CO_2. This standard was originally used by H. Urey and his colleagues at the University of Chicago (Craig 1957 and references therein). It has become a primary reference standard for expressing variations of carbon isotopes and those of oxygen

isotopes in carbonates and CO_2. Hut (1987) evaluated that PDB was enriched by 30.9‰ in ^{18}O with respect to V-SMOW.

The isotopic composition of light elements with more than one stable nuclide (such as oxygen and hydrogen) are variable because chemical and physical processes occuring in nature result in isotope fractionation. The fractionation is due to slight variations in the physical and chemical properties of isotopes and is expressed by the fractionation factor α which is defined as:

$$\alpha = \frac{R_A}{R_B} = \frac{\delta_A + 1000‰}{\delta_B + 1000‰} \qquad (2.2)$$

where R_A is the ratio of the rare to the abundant isotope in phase A and R_B is the same in phase B. The fractionation factor for any two phases is temperature dependent and generally approaches unity at increasing temperatures.

3

Methods

This chapter reports the progress made in applying the CO_2-H_2O equilibration technique to $\delta^{18}O$ analysis of water samples at the Insitut für Umweltphysik (IUP) in Heidelberg. An extensive analysis of the errors inherent to the original design of Finnigan MAT™´s auto-preparation device was followed by a few, inexpensive but effectful modifications which drastically improved the analytical precision. A modified preparation technique for very small samples (50-300µl) is also discussed. Both preparation methods allow automated equilibration, gas purification and mass spectrometric analysis in conjunction with the ISODAT™ software. The main advantage of the methods are minimal operator time, excellent analytical precision, and low cost.

This chapter also includes a section on cryogenic sampling of atmospheric moisture developed at the Institut für Umweltphysik, which will give an overview on different cold trap designs.

3.1 CO_2-H_2O Equilibration for ^{18}O Analysis of Water

Precise measurement of $\delta^{18}O$-values in water is generally based on the CO_2-H_2O isotope equilibration method first used by Epstein and Mayeda (1953). The high reproducibility and precision (±0.02‰) attainable by using this method has been documented in many studies on oceanic water (e.g. Craig & Gordon 1965).

3.1.1 Principle

The CO_2-H_2O equilibration proceeds via the hydration reaction of dissolved CO_2 in water. On the average three single reactions are necessary to exchange both oxygen atoms of a CO_2 molecule. Two reaction paths are important (Faurholt, 1924):

$$CO_2 + H_2O \Leftrightarrow H^+ + HCO_3^- \tag{3.1}$$

and

$$\begin{aligned} &CO_2 + OH^- \Leftrightarrow HCO_3^- \\ &H^+ + OH^- \Leftrightarrow H_2O \end{aligned} \tag{3.2}$$

The time required to achieve complete isotopic equilibrium depends on the rate of hydration and the rate of gas-water exchange. The gas exchange is the slow step but can

be speeded up by shaking the equilibration vials (Roether 1970). The gaseous CO_2 in equilibrium is enriched in ^{18}O compared to the water (α=1.04378 at 21°C; Brenninkmeijer *et al.* 1983).

Isotopic equilibrium between CO_2 and H_2O is reached under closed conditions. The overall isotopic composition of the system remains constant[1]. Measurement of the $\delta^{18}O$-value of the initial and the equilibrated CO_2 permits the calculation of the isotopic composition of the water sample:

$$\frac{a \cdot \delta^{18}O^{i}_{H_2O} + b \cdot \delta^{18}O^{i}_{CO_2}}{a+b} = \frac{a \cdot \delta^{18}O^{f}_{H_2O} + b \cdot \delta^{18}O^{f}_{CO_2}}{a+b} \qquad (3.3)$$

where the superscripts i and f indicate the initial and final equilibrium states; a and b represent the number of moles of oxygen in the water and the carbon dioxide phase. Equation (3.3) can be solved for the initial $\delta^{18}O$-value of the water sample:

$$\delta^{18}O^{i}_{H_2O} = \frac{b}{a} \cdot (\delta^{18}O^{f}_{CO_2} - \delta^{18}O^{i}_{CO_2}) + \delta^{18}O^{f}_{H_2O} \qquad (3.4)$$

In equilibrium the fractionation factor α is the isotopic ratio between the final isotopic compositions of CO_2 and H_2O. Substitution of $\delta^{18}O^{f}_{H_2O}$ with $\frac{1+\delta^{18}O^{f}_{CO_2}}{\alpha} - 1$ according to (2.2) in (3.4) gives:

$$\delta^{18}O^{i}_{H_2O} = \frac{b}{a} \cdot (\delta^{18}O^{f}_{CO_2} - \delta^{18}O^{i}_{CO_2}) + \frac{1+\delta^{18}O^{f}_{CO_2}}{\alpha} - 1 \qquad (3.5)$$

The $\delta^{18}O$-value of the water sample is then normalised to the SMOW-scale. This is achieved by applying a linear fit known from calibration of the method versus the international agreed standards V-SMOW and SLAP (Gonfiantini *et al.* 1995). This is an important step to obtain results which are not only internally consistent but also directly comparable with those obtained by other labs.

The stable isotope lab at the IUP in Heidelberg uses three internal standards with different isotopic compositions to continuously monitor results and mass spectrometer precision. I also considered an additional normalisation of each batch to one of the internal standards but I found that this method did not improve the analytical precision.

[1] Overall reaction: $C^{18}O^{16}O + H_2{}^{16}O \Leftrightarrow C^{16}O^{16}O + H_2{}^{18}O$

3.1.2 Experimental

At the IUP in Heidelberg, sample preparation is carried out on an automated equilibration device from Finnigan MAT coupled to a Finnigan MAT 252 mass spectrometer (Fig. 3.1). Up to 48 samples per day can be processed with only two hours of operator time. The device is based on Roether's (1970) design for an automated variant of the Epstein-Mayeda technique. It employs shaking of the equilibration vials to speed up the equilibration reaction. The equilibration vials are connected to the vacuum line via capillaries to enable the removal of air from the headspace without the need to freeze the water prior to pumping. The purity of the gaseous CO_2 is important to the analytical precision of the mass spectrometric measurement. Any sample gas admitted to the mass spectrometer is therefore checked for mass 40 (argon) after measurement.

The equilibration units were significantly improved by Rolf Neubert and Christel Facklam who installed new temperature controls for the water baths (better than ±0.05K, Neubert 1998). Electrically operated lifts for the two vacuum lines facilitate the handling of the samples. The system achieved a routine precision of ±0.05‰ but repeated analysis of internal standards revealed fluctuations of up to 0.12‰ within two years. The application of isotopic tracers in ice cores from polar and alpine glaciers and in open ocean studies require a higher degree of reproducibility and a routine precision of ±0.02‰ or better. It has been a key requirement of this work to further improve analytical precision and long-term reproducibility.

Brenninkmeijer and Morrison (1987) developed a similar automated system in which air is removed from the equilibration vessels by quickly pumping und flushing with CO_2 for three times. More recently, several labs have begun to use pre-evacuated glass vials, injecting both the H_2O and CO_2 into the vial (Socki et al. 1992). However, none of the systems have achieved routine precisions to better than ±0.05‰. At that time, it seemed that a time-consuming "freezing over" was an essential step in sample preparation for precise $\delta^{18}O$ determinations of natural waters.

This equilibration device (Fig. 3.1) consists of two independent units with 3 manifolds à 8 sample ports. The two separate water baths have individual temperature controls (HAAKE F3) with a common cooling unit. The water of each bath circulates through the temperature control unit once per minute. The manifolds and the cold trap are pumped by an EDWARDS E2M5 two stage rotary pump to a pressure of 0.2 Pa ($2 \cdot 10^{-3}$mbar). The entire construction is made of stainless steel. All valves are electrically operated and controlled by ISODAT (V 5.1) software from Finnigan. The cold trap is cooled with an acetone/dry ice slush. The vials (ca. 22.7 ml in volume) are made from standard boro-silicate glass with DIN[2] 14 (GL) threads. Each vial is labelled and calibrated for volume by weighing dry and water filled.

Samples are prepared in batches of 16, 24 or 40. The vials are filled with 5 ml water and attached to the capillaries (Fig. 3.2b). The original seals from Finnigan were replaced by viton O-rings. Within one batch, each bank contains one standard. A lift immerses the vials into the water bath (21°C) and the shaker (ca. 2 Hz) is started. Vacuum pumping the vials for 20 minutes effectively removes any air in the headspace or dissolved in the water. This procedure also produces an isotopic enrichment of the water of approximately 0.07‰ in $\delta^{18}O$ due to evaporative loss of a small percentage of the sample. However, this systematic deviation does not necessarily affect analytical precision as long as pumping time is the same for calibration and routine analyses and the appropriate correction is applied.

The vials are then filled with CO_2 from a gas cylinder to a pressure of approximately 90 kPa (filling time 120 seconds). Pressure measurement is by a 3½ digit vacuum barometer. Neubert (1998) showed that CO_2 and H_2O equilibrate within 2.5 hours. In order to achieve the highest degree of reproducibility, all samples are allowed to equilibrate for 6 hours.

There exists a small residual gas volume between each capillary and its valve. The CO_2 in that residual volume has not exchanged oxygen atoms with the water and is therefore pumped away by opening each valve for one second. The equilibrated CO_2 is then expanded from the equilibration vial into the vacuum line for 30 seconds. The cryogenic trap cooled with a dry ice/acetone slush removes any water vapour in the gaseous CO_2. The expansion volume is approximately 370 ml and provides sufficient gas for a standard, non-cold finger[3] mass spectrometer run.

[2] DIN, Deutsches Institut für Normierung (German Institute for Standardisation)

[3] Cold finger: Some mass spectrometers provide a small cold trap cooled with liquid nitrogen in order to collect all available CO_2 prior measurement.

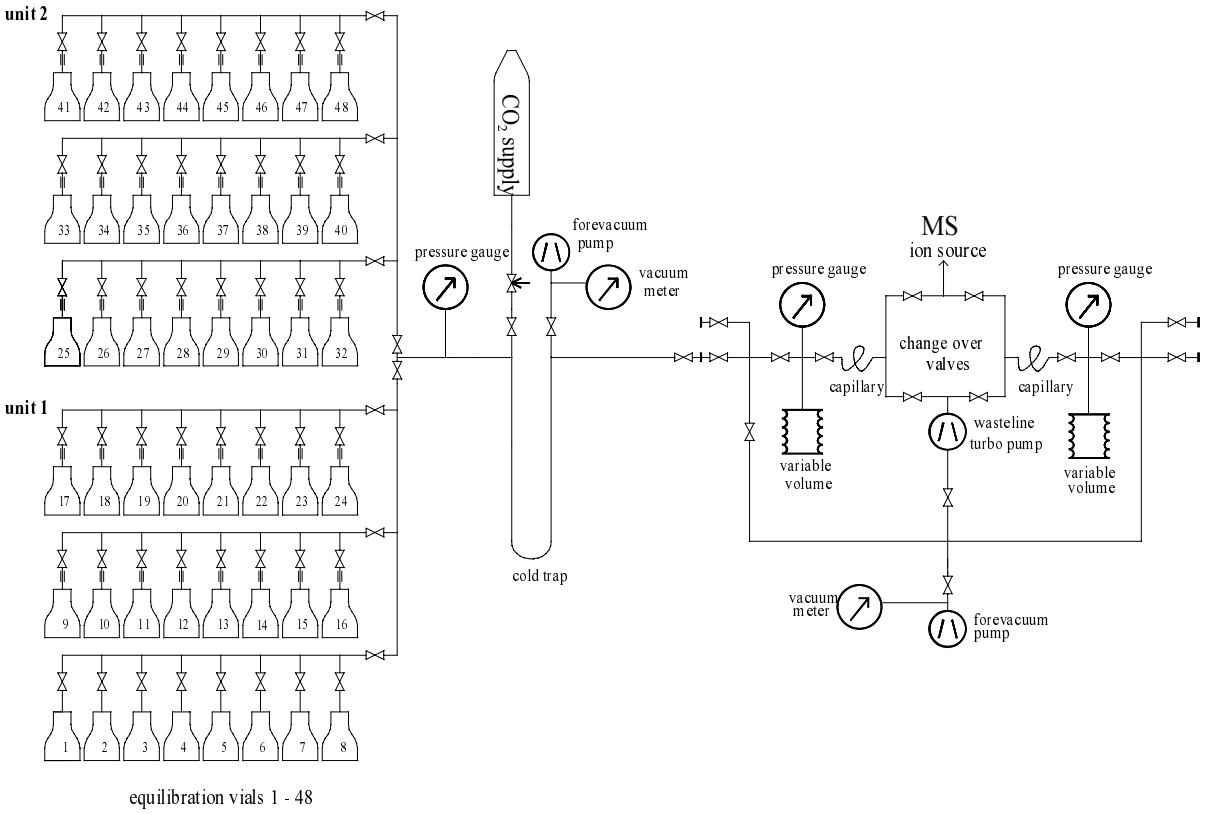

Fig. 3.1 Sketch of the H_2O-CO_2 equilibration device and the inlet system of the MAT 252 mass spectrometer. Equilibration vials at ports 9 to 48 are connected to the vacuum line via capillaries. Ports 1 to 8 are without capillaries for small sample volumes.

3.1.3 Optimisation

The optimisation of the CO_2-H_2O equilibration device started with a rigorous analysis of the source and magnitude of errors associated with each term in (3.5). The number of moles of oxygen in the water, **a**, is given by dividing the sample volume by 18ml, the molar volume of water. The precision of delivery of the pipette used, and hence the relative precision in **a** is ±0.7%. The number of moles of oxygen in CO_2, **b**, is determined using the gas equation:

$$\mathrm{b} = 2\mathrm{n} = 2 \cdot \frac{PV}{RT} \tag{3.6}$$

where n is the number of moles of CO_2, V is the volume of CO_2 (m^3), P is the gas pressure (Pa), R is the gas constant ($JK^{-1}mol^{-1}$), and T is the absolute temperature (K). V

is determined by subtracting the water volume (5ml) and the volume of the tip of the port (0.22ml) from the volume of the equilibration vial (ca. 22.7 ml). The volume of each vial used has been determined to ±0.3%. The original pressure gauge had a precision of only ±5% and was replaced by a 3½-digit manometer with a precision of ±0.1%. Temperature has been checked with a mercury thermometer to better than ±0.05K.

Combining all contributing errors of **a** and **b** results in a negligible total error. The dimension less term **b/a** in (3.5) is approximately $6 \cdot 10^{-3}$, and the difference between final and initial $\delta^{18}O$ of the CO_2 in the vial is generally less than 35‰, in the case of seawater samples it is even less than 2‰. Thus, all uncertainties associated with the term **b**/**a** cannot affect the derived water $\delta^{18}O$ composition by more than ±0.002‰.

Due to the temperature dependence of the fractionation factor α, an increase of only 0.1K causes an isotopic depletion in the gaseous CO_2 of 0.02‰. Thus, great care is necessary to ensure that no temperature fluctuations disturb the equilibration process. Although the new temperature control minimises temperature fluctuation of the water bath to ±0.05K or less, condensation occured frequently in the headspace of the equilibration vials indicating a temperature gradient inside the vial. The problem was caused by a flow of cold air from the air conditioning outlet. A simple cover made from plastic foil resolved the condensation problem but did not improve the analytical precision to a great extent.

Having eliminated any errors associated with (3.5), the optimisation strategy focused on the capillaries. Weighing samples of identical isotopic composition before and after pumping air out of the equilibration vials revealed considerable variations in the water loss (26 ± 12mg) which were correlated with the measured $\delta^{18}O$-values (Fig. 3.2). Furthermore, it was frequently noticed that offsets in $\delta^{18}O$ occured repeatedly at the same ports with the same capillaries. Careful examination of the capillaries often revealed tiny deformations at the endings or dirt sitting inside. Both occurrences reduce the flow rate through the capillary and need to be avoided.

Ultrasonic and mechanical cleaning[4] of capillaries and manifolds enhanced precision but much better results were obtained after complete replacement of the existing capillaries by ones manufactured in the workshop of the IUP. The capillary (outer/inner diameter: 0.55/0.30mm) is placed in the centre of a 60mm long 0.25 inch stainless steel tube, as illustrated in Fig. 3.3a. Both ends of the tube are welded to the capillary. The end attached to the vial is polished flat. The new capillaries have four major advantages over the old capillaries:

[4] mechanical cleaning: inserting a fine stainless steel capillary into the other capillary.

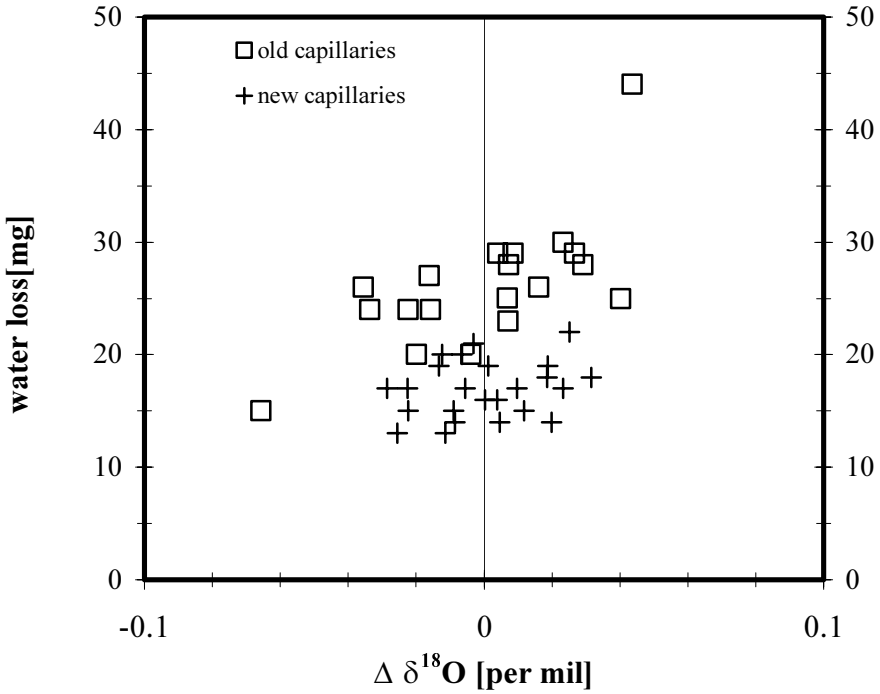

Fig. 3.2 Evacuation of the equilibration vials at 21°C results in a partial loss of water and isotope fractionation. The plot shows water loss and deviation of the $\delta^{18}O$ value after correction for 20 minutes vacuum pumping.

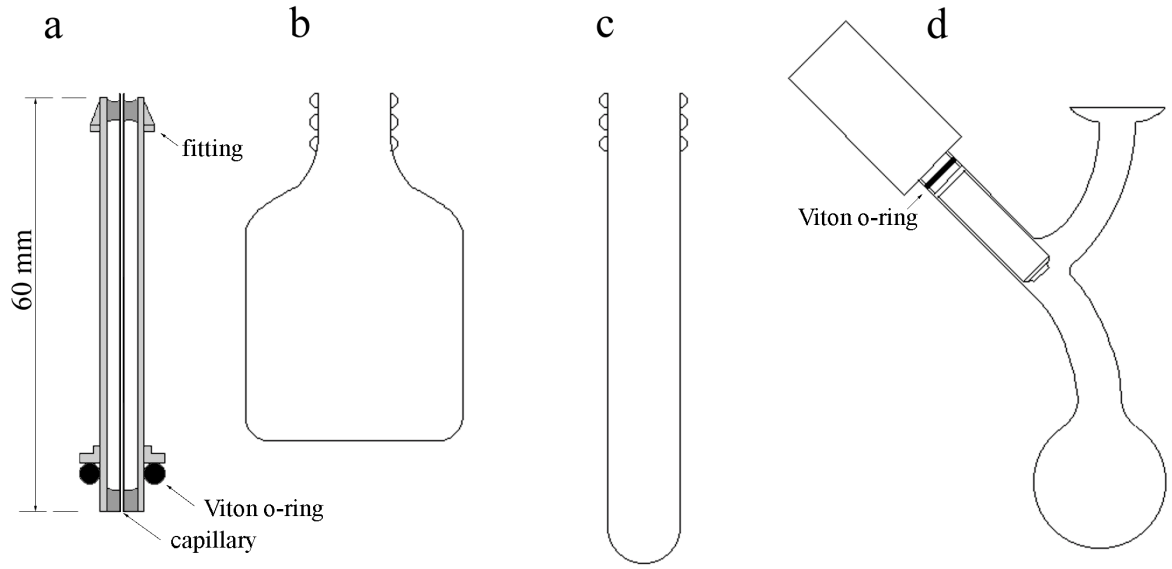

Fig. 3.3 (a) improved capillary port for 5ml sample preparation. The lower ending is polished flat and connects to the vial. The upper ending connects to the valve with a SWAGELOCK® fitting. **(b)** standard vial (boro-silicate glass with thread) used for all samples from 100µl to 300µl and 5 ml, **(c)** vial (boro-silicate glass with thread) for 50µl samples, **(d)** vial (boro-silicate glass) with GE valve for 50µl to 300µl samples. Here, the upper teflon O-ring has been replaced by a viton O-ring for improved sealing when samples are frozen.

⇛ No capillaries extend out of the tube. Those used to leave marks on the operator's hands. Thus, fragments of human skin cannot plug up the capillaries.
⇛ Both endings of the capillary have an ideal shape and are protected from any deformation.
⇛ The residual volume between valve and capillary has been greatly reduced since both endings are welded.
⇛ All capillaries have exactly the same length.

The new capillaries ensure a higher degree of reproducibility of water loss during vacuum pumping, as can be seen from Fig. 3.2. Note that the average water loss was reduced from 26ml to 17ml. However, the capillaries require a minimum of maintenance. Especially when sea water is analysed, it is recommended to clean manifolds and capillaries on a regular basis. Otherwise small salt crystals may clog the capillaries again.

The modifications to the Finnigan equilibration device may seem small but proved to be very effective. The analytical precision and long-term reproducibility improved to just ±0.025‰ for internal lab standard Meteor 23-4, Fig. 3.4.

The installation of a new ion source into the Finnigan MAT 252 mass spectrometer in March 1999 further enhanced analytical precision. The external reproducibility[5] of the mass spectrometer improved from ±0.025 to ±0.018‰ for $\delta^{18}O$. The reproducibility of $\delta^{18}O$ measurements in water increased to ±0.017‰ for lab standard Meteor 23-4 and its successor Me 56. The measured $\delta^{18}O$ values of lab standard Meteor 23-4 and its successor Me 56 are normally distributed about the mean with a 1σ precision ±0.017‰, Fig. 3.5(a+b).

Only lab standard Groenland B-26 has a poorer reproducibility of ±0.030‰. The histogram in Fig. 3.5(c) reveals a distribution of $\delta^{18}O$ values about the mean with a tail towards heavier isotope compositions. This indicates that one source of error results in a bias of the measurement of $\delta^{18}O$ in Groenland B-26. There are two plausible explanations: (i) The error associated with term b/a could be larger than presumed. Changes in b/a affect measured $\delta^{18}O$ in Groenland B-26 twice as much as in Me 56 or Meteor 23-4, due to the larger shift in $\delta^{18}O$ of CO_2 during equilibration. (ii) There could be a small memory effect in the ion source because CO_2 equilibrated with Groenland-B26 is 31.8‰ lighter than standard reference 'Meerwasserstandard' (gas standard) which is CO_2 equilibrated with seawater and therefore in its isotopic composition very close to CO_2 equilibrated with Me-56 or Meteor 23-4. If isotope

[5] long term reproducibility of one gaseous lab standard vs. a second lab standard, in this case ‚Pflanzenstandard' vs. ‚Oberlahnstein' which differ by 12.20‰ in $\delta^{18}O$ (see also Neubert, 1998 chapter 5).

ratios of sample and reference gas deviate a lot from each other, then cross contamination in the ion source can occur when the change over valves switch from sample to reference gas and vice versa. The effect on analytical precision can be demonstrated when gas standards of widely varying oxygen isotope compositions are measured against each other, Fig. 3.6(a,b). The gas standards "Oberlahnstein" and "Reinst" deviate by more than 25‰ from each other. Measurements of "Oberlahnstein" versus "Reinst", Fig. 3.6(a), display a less ideal data distribution and a higher 1σ value than the measurements of "Pflanzenstandard" versus "Oberlahnstein", Fig. 3.6(b), which deviate only by 12‰.

However, the choice of reference gas is optimized for seawater samples where the total range of $\delta^{18}O$ is small (1-2‰) requiring an analytical precision of better than ±0.02‰.

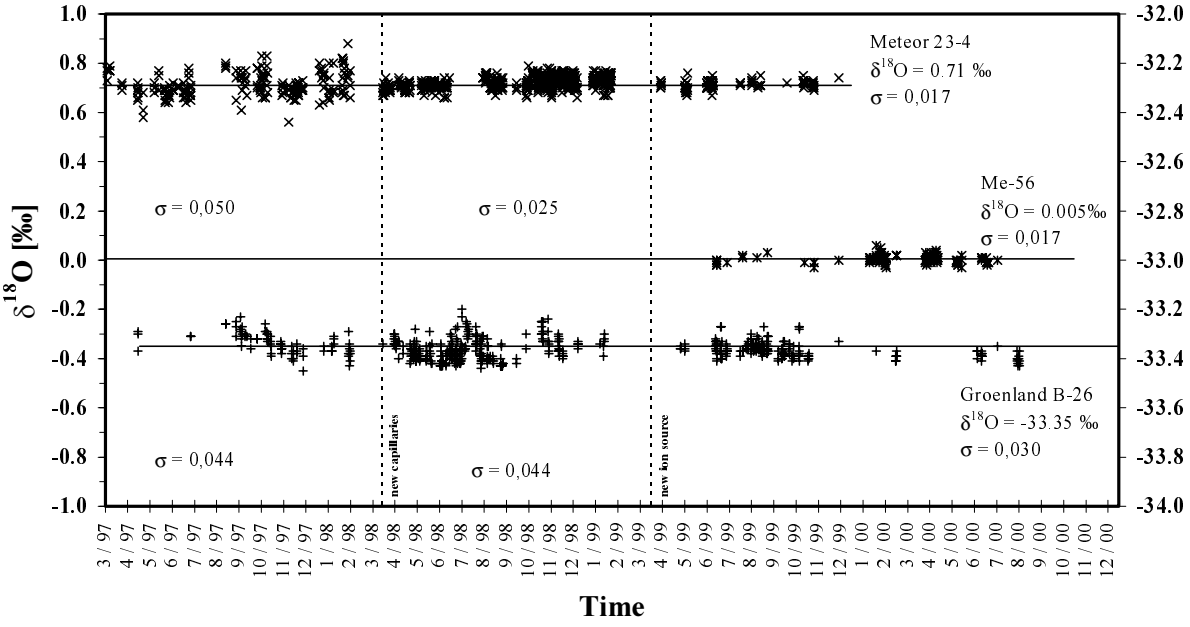

Fig. 3.4 Three internal water standards (Meteor 23-4, Me-56, and Groenland B-26) have been used to determine the precision and reproducibility of the CO_2-H_2O equilibration technique. The plot shows all measurements of these standards since March 18 1997. Meteor 23-4 (798 analyses, now out of stock) and its successor Me-56 (116 analyses) are destilled sea water, whereas Groenland B-26 has been derived from precipitation of Greenland (554 analyses). The vertical dashed lines mark the improvements (new capillaries, new ion source) of the facilities.

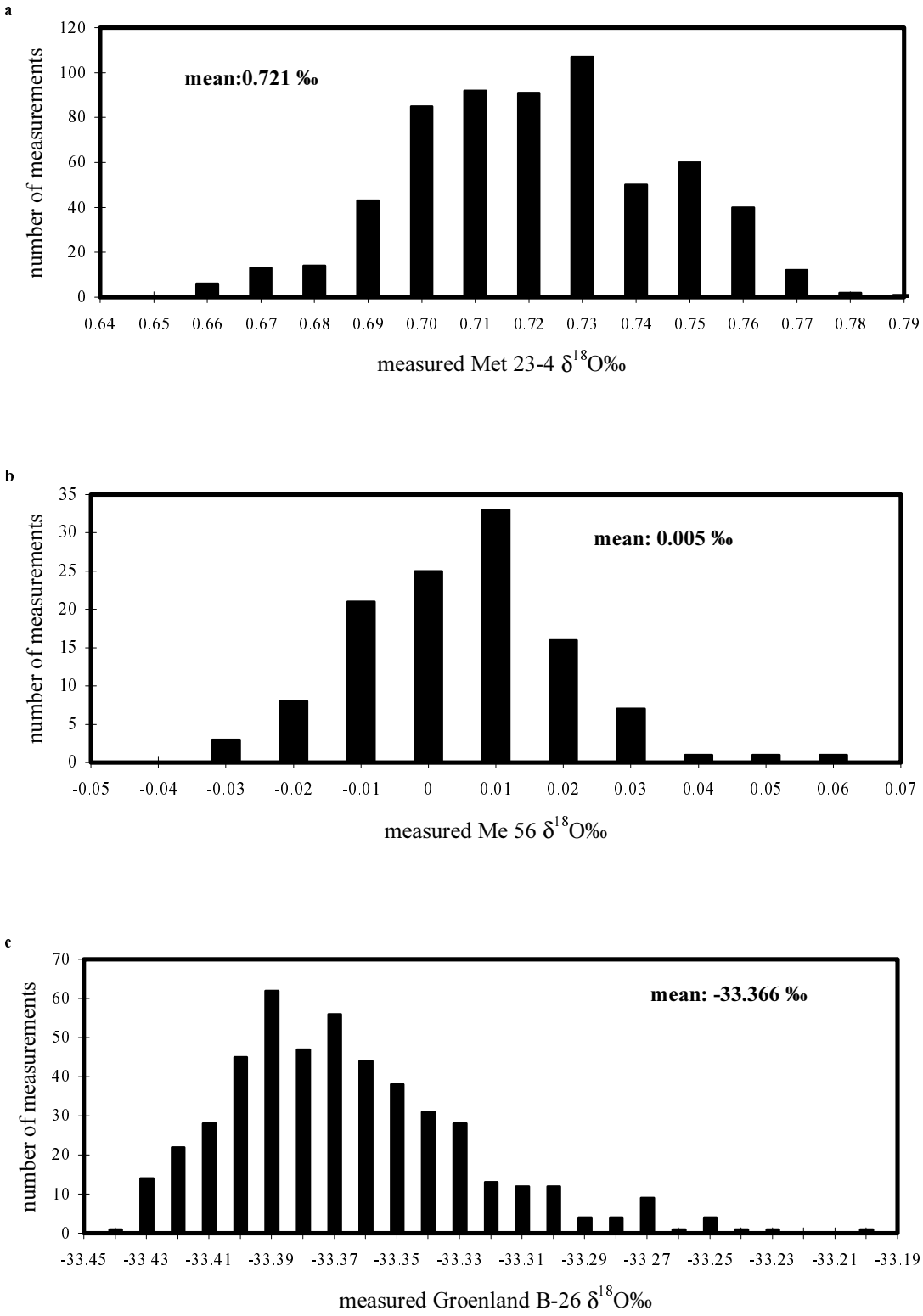

Fig. 3.5 (a-c) Results of 516 analyses of the Met 23-4 standard, 116 analyses of the Me 56 standard, and 478 analyses of the Groenland B-26 standard since 30th March 1998.

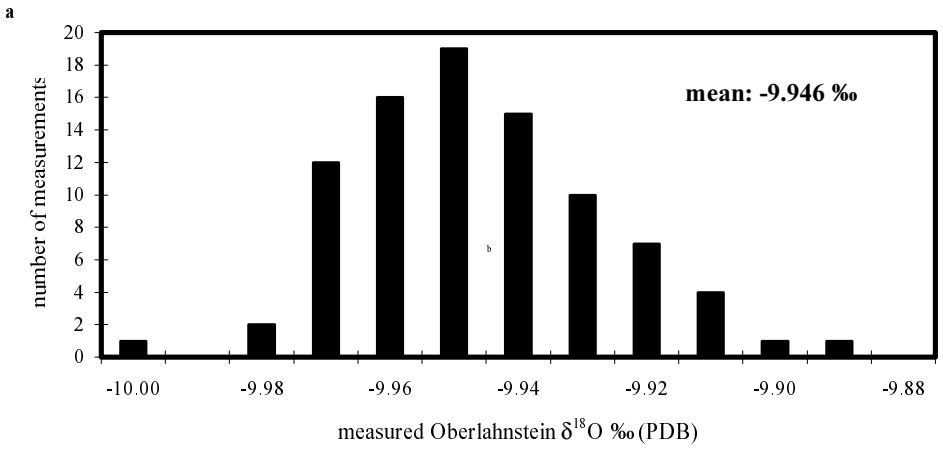

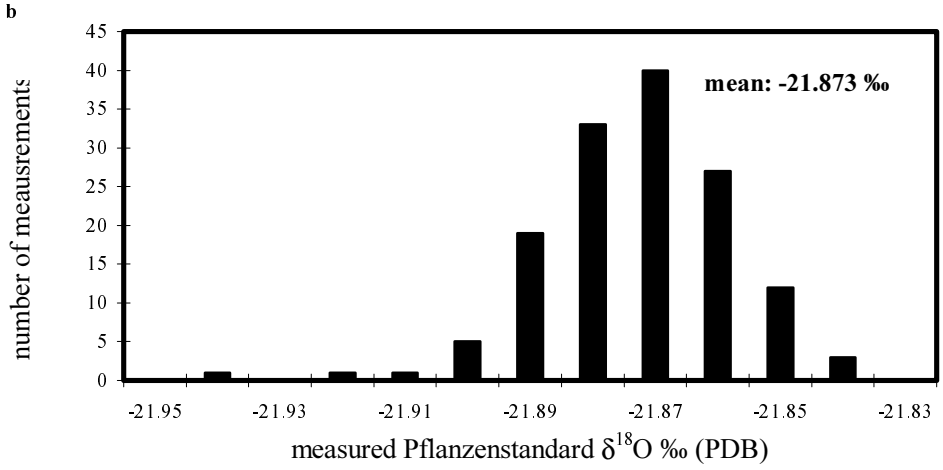

Fig. 3.6(a) The histogram plot of 88 analyses of gas standard "Oberlahnstein" vs. gas standard "Reinst" shows a non-normal distribution about the mean –9.946 ± 0.019‰. The plot **(b)** with 141 analyses of gas standard "Pflanzenstandard" vs. "Oberlahnstein" shows a near normal distribution about the mean –21.873 ± 0.015‰. (Explanation see text)

3.1.4 International comparison

In 1998/1999, the IAEA hydrology section organised the second interlaboratory comparison test for analyses of oxygen and hydrogen stable isotope composition of water samples (Lippmann *et al.* 1999). This test allowed stable isotope labs around the world to assess their precision and accuracy for the range of $\delta^{18}O$ and $\delta^{2}H$ values normally observed in meteoric waters.

Each participating lab received four water samples for analysis and a reporting sheet for details of their sample preparation. The labs were requested to report their δ-values on the normalised VSMOW-SLAP scale. A selected group of seven well-reputed labs was assigned to provide the consensus values for the analysed set of

samples. 80 participating labs reported their $\delta^{18}O$ values for the set of four samples. 75 labs reported $\delta^{2}H$ values for the comparison project.

The stable isotope lab at the IUP analysed each sample four times. The $\delta^{18}O$ values reported by IUP deviate no more than ±0.01‰ from the consensus values. Thus, the results of the IUP are within the range of uncertainty of the consensus values given by the IAEA itself. It is interesting to note that the IAEA samples were analysed before the new ion source further improved the analytical precision. The δD results of the IUP are 1.2 to 1.5‰ higher than the consensus values and the standard deviation is quite large. However, the setup of the hydrogen preparation line has changed since this comparison to place and most recent results are very promising.

Table 3.1 summarises the results obtained by the selected group (IAEA), the stable isotope lab of the Institut für Umweltphysik, and the mean of all participating labs.

Roether's (1970) design of a CO_2-H_2O equilibration device has long been considered as inferior to the conventional "freezing over" technique when ultimate analytical precision is demanded. This work and the results of the IAEA interlaboratory comparison test prove that fast and convenient sample preparation does not need to sacrifice analytical precision.

Tabelle 3.1 Summary statistics of the results obtained by the reference labs (IAEA values), the stable isotope lab of the Institut für Umweltphysik (IUP Heidelberg values), and all participating labs.

Sample	OH – 1	OH – 2	OH – 3	OH – 4
	mean ± stdev	mean ± stdev	mean ± stdev	mean ± stdev
$\delta^{18}O$ [‰]				
IAEA	-0.05 ± 0.01	-3.28 ± 0.01	-8.65 ± 0.02	-15.28 ± 0.01
IUP Heidelberg	-0.04 ± 0.02	-3.28 ± 0.02	-8.64 ± 0.02	-15.27 ± 0.02
All labs	-0.10 ± 0.21	-3.33 ± 0.23	-8.68 ± 0.20	-15.34 ± 0.20
$\delta^{2}H$ [‰]				
IAEA	-3.9 ± 0.2	-30.8 ± 0.2	-61.3 ± 0.2	-109.4 ± 0.2
IUP Heidelberg	-2.7 ± 0.7	-29.5 ± 1.0	-60.1 ± 0.8	-107.9 ± 0.4
All labs	-4.2 ± 2.0	-31.5 ± 1.8	-61.8 ± 2.1	-110.0 ± 2.1

Data have been taken from the IAEA-report "2nd Interlaboratory Comparison for Deuterium and Oxygen-18 Analysis of Water Sample" by Lippmann *et al.* (1999).

3.1.5 Preparation of Small Water Samples for ^{18}O Analysis

Sampling of air moisture is often limited to milligram quantities of water. Either because humiditiy is extremely low like it is in the stratosphere/tropopause region, or a high temporal resolution is desired (Zahn *et al.* 1998). The standard equilibration device by Finnigan is not suitable for samples below 2g because vacuum pumping will alter the isotopic composition of the sample too much.

The sample preparation technique for tiny sample amounts developed at the IUP is based on the conventional CO_2-H_2O isotope equilibration method first used by Epstein and Mayeda (1953) and includes the freezing of the water sample at liquid nitrogen temperature prior to evacuation.

This approach yields the best analytical precision for water samples as small as 50µl. However, the analyses require correction for equilibrium and evaporation isotope effects differing from large sample preparation (see above). 8 capillary ports of equilibration unit 1 were replaced by 0.25 inch stainless steel tubes for rapid vacuum pumping. Different vials have been tested for small sample sizes.

First experiments used reaction vessels where samples were injected through a septum in the pre-evacuated equilibration vessels by means of a syringe. Unfortunately, it turned out that CO_2 exchanged with H_2O adsorbed to the septum and erratic isotopic compositions were obtained.

Several tests were performed with small vials of 5ml volume and 7cm length with a rounded bottom, Fig. 3.3(c). The sample is delivered to the bottom of the vial by a small syringe. The vials worked for 50µl and 100µl sample quantities. Larger samples, however, yielded sporadically erratic isotopic compositions. It turned out that freezing and subsequent degasing of the liquid sample sometimes spatters small drops to the top of the vial. This phenomenon is fostered by the small round bottom of the vial. Therefore, standard vials, Fig. 3.3(b), with a volume of 22.7 ml are used if samples are larger than 100µl. In this case, CO_2 pressure is reduced to 500 hPa.

A different vial design is shown in Fig. 3.3(d). The expanded volume at the bottom prevents any spattering during freezing. The stop cock (Glas Expansion) was intended to avoid an isotopic exchange with air moisture. In practice, however, no improvement in precision was accomplished. In order to keep operator time at a minimum, standard vials are most frequently used.

The small sample size slows down equilibration between CO_2 and water because it decreases the ratio of CO_2 dissolved in the water phase to total CO_2 in the system. If less CO_2 is dissolved at a time, the throughput of the reaction path is reduced and more time is required to achieve complete isotopic equilibrium. Furthermore, gas exchange with a rigid drop is much slower than across an agitated interface (Roether 1970). Preliminary tests suggested that 100 µl of water at 21°C equilibrate with 5-6 ml CO_2 at 900 hPa within 26 hours. The analysis of internal lab standards revealed a 1σ precision

of ±0.1‰. Repeated tests with longer equilibration times (2 days) improved the precision to ±0.03‰. Obviously, the speed of equilibration of small water samples was previously overestimated.

Recent measurements of lab standards Me 56 ($\delta^{18}O$=0.05‰) and HD-VE 95 ($\delta^{18}O$=–8.70‰) as 100µl quantities confirm the excellent reproducibility with mean compositions of 0.05±0.02‰ and –8.70±0.03‰, respectively (Fig. 3.7). The isotopic composition of these lab standards has been been determined by more than 100 routine analyses (standard preparation with 5 ml).

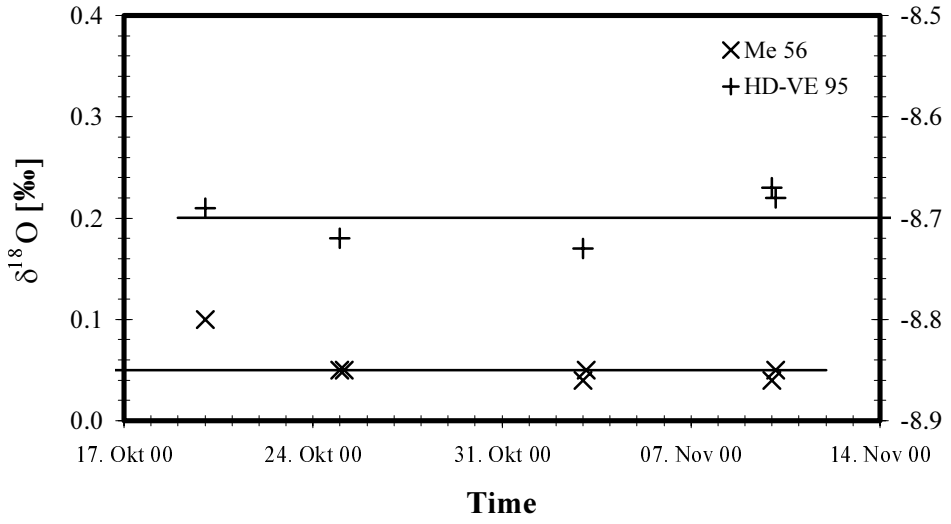

Fig 3.7 Two lab standards (Me-56 and HD-VE 95) have been used to determine the precision and reproducibility of the CO_2-H_2O equilibration technique for small sample sizes. The plot shows seven measurements of Me 56 and five measurements of HD-VE 95 with mean compositions of 0.05±0.02‰ and –8.70±0.03‰, respectively.

3.2 Conversion of Water by F_2 for Triple Oxygen Isotope Analysis

Regarding the H_2O-CO_2 equilibration method, it should be pointed out that the transfer of the isotopic composition from H_2O to CO_2 obstructs the measurement of $\delta^{17}O$. The molecule species $^{12}C^{16}O^{17}O$ and $^{13}C^{16}O^{16}O$ have the same mass (m = 45) within the precision of mass spectrometric measurements. Because ^{13}C is 29 times more abundant than ^{17}O any attempt to correct mass 45 for ^{13}C will result in poor analytical precision. Although it is conceivable to use pure $^{12}CO_2$ for equilibration, the sensitivity of the collector unit for mass 45 must be adjusted to lower ion currents. This would require a complete re-calibration of the mass spectrometer each time the setup is changed from $\delta^{17}O$ to $\delta^{13}C$ and vice versa.

The interest in $\delta^{17}O$ has been triggered by the discovery of mass independent fractionation in several atmospheric trace gases such as O_3, CO, CO_2, and N_2O. It is

assumed that stratospheric water vapour shows a mass independent $\delta^{17}O$ signal, too (Bechtel & Zahn *submitted*). This is in contrast to tropospheric water vapour and to all other terrestrial matter where the two oxygen isotope ratios $^{18}O/^{16}O$ and $^{17}O/^{16}O$ are mass-dependently correlated: i.e. $\delta^{17}O$ values are approximately 0.52 times $\delta^{18}O$ values (Robert *et al.* 1992).

A robust preparation technique for $\delta^{17}O$ and $\delta^{18}O$ in tiny water samples is described by O'Neil and Epstein (1966): 20 mg of water react with BrF_5 to O_2 and HF in a nickel reaction vessel at 150°C. The released oxygen is purified cryogenically and analysed in a dual inlet IRMS. O_2 can be trapped on silica gel at liquid nitrogen temperature before it is admitted to the IRMS (Mattey, 1997 *pers. comm.*).

The IUP in Heidelberg planned a similar preparation line. In order to improve safety for the operator, a substitution of BrF_5 with less dangerous fluorine was proposed. Fluorine of high purity can be generated from $K_2NiF_6 \cdot KF$ at 400°C (Asprey 1976). Water reacts with fluorine in a nickel or Kel-F[6] recation vessel. The loading of the water sample should prevent the contact of liquid water with the inner vessel surface. The design of the reaction vessel is therefore most critical to the complete setup. A possible design of the preparation line and the reaction vessel is illustrated in Fig. 3.8. The reaction vessel includes a loading system developed by Elena Dubinina (Dubinina, 1997 *pers. comm.*) which allows sample sizes down to 3 µl.

Although reaction takes place at room temperature, several oxy-halogen compounds may form which decompose at higher temperatures. Thus, the reaction vessel should be heated to 150°C. The analytical precision of this approach can be expected to be better than ±0.2‰.

The setup of lab facilities for oxygen triple isotope analysis were financially and strategically linked to a research proposal for balloon borne stratospheric air sampling. Since this proposal was rejected in 1998, a less expensive alternative based on the conventional CO_2-H_2O isotope equilibration method needed to be planned.

[6] Nickel and the flouro-plastic Kel-F resist F_2 – boro-silicate glass would be destroyed.

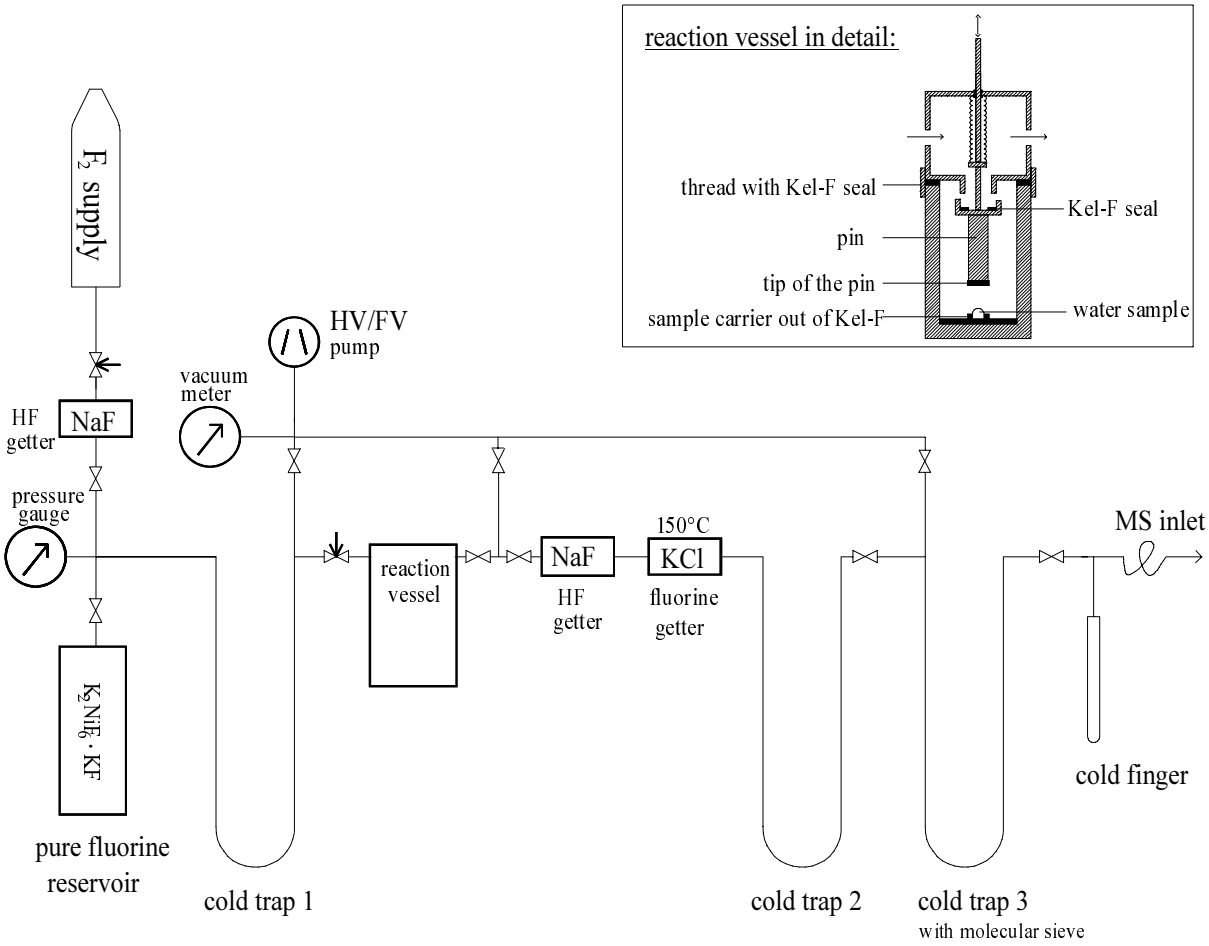

Fig. 3.8 Preparation line for triple oxygen isotope measurements in water. A small trop of water is placed with a syringe into the reaction vessel which is then mounted to the vacuum line.

3.3 Air Moisture Sampling

In order to trace the isotopic variability of atmospheric moisture, a suitable sampling technique is required. There is a large number of different methods and designs in the literature. Most common is the use of a cryogenic trap cooled with an acetone/dry ice slush (Schoch-Fischer *et al.* 1984, Wang & Yakir 2000 and references therein), but other methods based on chemical or physical absorbers have also been introduced in literature (Soyez 1999, Thoma 1979).

Any sampling technique must be optimized for attaining quantitative trapping because an incomplete recovery changes the original isotopic composition.

A simple approach uses a glass trap with several loops over a central arm which is also the inlet. The central arm has a greater diameter than the loops because most of the moisture accumulates within the first few centimeters and any clogging by ice must be prevented. In addition, glass wool or, even better, sintered glass is fitted below the

outlet to prevent the escape of small flakes. These flakes may form when supersaturation occurs not only at the inner wall but also at other locations in the trap. It also happens that small flakes on the surface are pulled off by air friction. This classic design has excellent trapping efficiencies and was used with an acetone/dry ice slush for standard tests in the lab.

An alternative cold trap design consists of two (or more) concentric tubes. This design is more practical for frequent trap swapping and limited space because no fragile loops are required. The concentric arrangement permits heat exchange between the cold air at the outlet and the warm air at the inlet, which reduces the consumption of coolant. The design in this study has been optimized for limited space and coolant consumption. It includes an accumulation reservoir to prevent clogging by ice and a special heat exchange section with undulations to improve cooling. The filter is made out of sintered glass with a pore size of 16-40 µm and is placed in the middle to minimize re-evaporation of flakes.

Cold traps of this kind have been used with an acetone/dry ice slush for short-term sampling of ambient air moisture, Fig. 3.9 (see also section 5.3).

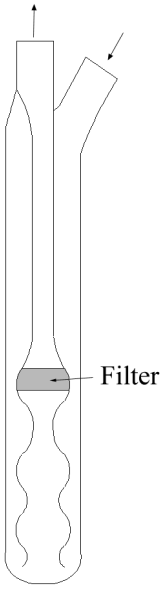

Fig. 3.9 Cold trap for water samples < 0.5 g. Length: 12cm.

The water vapour collection programme at Heidelberg uses yet another type of cryogenic trap. It also consists of two concentric tubes, but ambient air is introduced into the inner tube, as can be seen in Fig. 3.10. Electric heating is applied to the inner tube to prevent clogging by ice. The cooling is maintained by a commercial, electrically operated one-step cooling unit. The working temperature used to be -47°C/-50°C in the beginning of the record, but has increased to -44°C due to degradation over the years. If the water vapour collection programme is to be continued, a new cooling unit is needed

soon. The residual saturation water vapour pressure results in incomplete recovery, leading to isotopic enrichment of the sample. Thus, the isotopic composition of the sample must be corrected with an appropriate correction term. If the water vapour in the cold trap follows a Rayleigh condensation process, the appropriate correction term is:

$$\Delta\delta = \delta_{sample} - \delta_{air\ moisture} = (1-\alpha) \cdot F \cdot \ln(F) \qquad (3.7)$$

where α is the equilibrium fractionation factor and F is the fraction of the vapour lost during sampling (Schoch-Fischer et al. 1984). The internal heating is somewhat counterproductive but the configuration of the outlet and the tube length ensures that the air is indeed cooled down to the lowest possible temperature. This is essential because correction term $\Delta\delta$ is temperature dependent. However, the calculation of the correction term contains some uncertainties:

The solid/vapour equilibrium fractionation factors for ^{18}O and ^{2}H have not been tested for such low temperatures. Values for α have been reported for –40°C to 0°C (Majoube 1971a, Merlivat & Nief 1967) and must be extrapolated for lower temperatures.

Schoch-Fischer *et al.* (1984) report a precision of ±1.1‰ for $\delta^{18}O$ and ±2.8‰ for δD. Three recent comparison tests have been conducted to re-assess the precision of the sampling technique. An additional cold trap cooled with a dry ice/acetone slush has been used parallel to the existing cold trap in the cooling unit. The air sample has been split for the two cold traps and the isotope analyses revealed a 1σ value of ±0.31‰ for $\delta^{18}O$ and ±3.6‰ for δD.

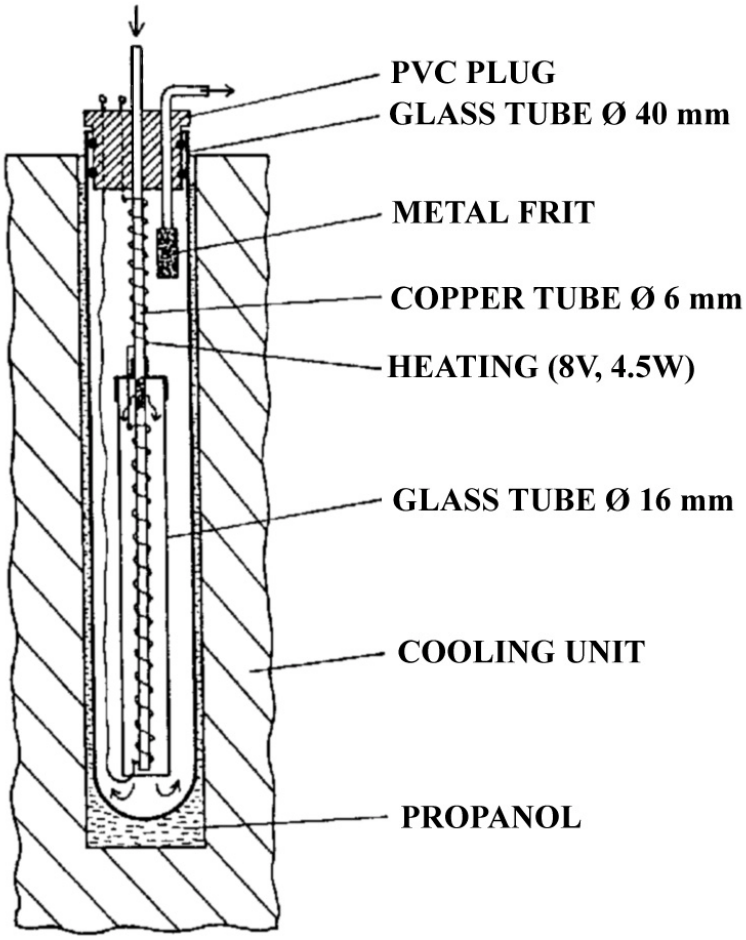

Fig. 3.10 Cold trap for continuous collection of atmospheric water vapour in an electrically operated one-step cooling unit. (Source: Schoch-Fischer *et al.* 1984)

4

Isotope Fractionation Accompanying the Hydrologic Cycle

The fractionation of oxygen and hydrogen isotopes in the form of different water molecules during evaporation and condensation is an important phenomenon. Compared to sea water, atmospheric water vapour is depleted in heavy isotopes. The depletion in the heavier isotopes increases with increasing degree of rainout of an air mass according to the Rayleigh formula. The average isotopic composition of precipitation takes an intermediate position between average atmospheric water vapour and sea water.
Evaporation into undersaturated air is accompanied by kinetic fractionation due to different molecular diffuisivities of the isotopically labelled water molecules. This effect changes the relation between oxygen and hydrogen isotopes in the vapour phase and can be used to trace local conditions at source regions of the vapour.

4.1 Equilibrium Fractionation

When water evaporates from the surface of the ocean, the water vapour is depleted in heavy isotopes compared to the liquid phase because $H_2{}^{16}O$ has a higher vapour pressure than $H_2{}^{18}O$ or HDO (vapour pressure isotope effect, v.p.i.e.). Consequently, the $\delta^{18}O$ and δD values of water vapour in the atmosphere are both negative. The fractionation factor α is related to the isotopic composition of water vapour, liquid water, and ice in the following way:

$$\alpha_{l\text{-}v} = R_l/R_v = (\delta_l + 1000)/(\delta_v + 1000) \tag{4.1}$$

or

$$\alpha_{s\text{-}v} = R_s/R_v = (\delta_s + 1000)/(\delta_v + 1000) \tag{4.2}$$

where R is the $^{18}O/^{16}O$ or D/H ratio. The subscripts l, s, and v refer to the liquid, solid, and vapour phase, respectively. The values of the isotopic fractionation factors for the evaporation and condensation of water under equilibrium conditions are strongly

dependent on temperature. The temperature dependence of the equilibrium isotope fractionation factors has been explored in numerous studies (see Table 4.1). The most accepted α values for hydrologic applications are those of Majoube (1971), Horita & Wesolowski (1994), and Merlivat & Nief (1967) which have been estimated in experiments with non-enriched waters. Jakli & Staschewski (1977) calculated α from the vapour pressure difference between $H_2{}^{16}O$ and highly enriched $H_2{}^{18}O$ measured directly with a differential manometer.

Table 4.1 Temperature dependence of the equilibrium isotope fractionation $\varepsilon = \alpha - 1$ for deuterium and oxygen-18. The values $\alpha_{s\text{-}v}$ are in italics.

Equilibrium isotope fractionation (‰)		**Temperature (°C)**								
		-30	**-20**	**-10**	**0**	**5**	**10**	**15**	**20**	**25**
Majoube (1971a,b)										
$\varepsilon_{18} = (\alpha_{s\text{-}v}\text{-}1)\cdot 10^3$	(1)	*20.7*	*18.7*	*16.9*	*15.2*					
$\varepsilon_{18} = (\alpha_{l\text{-}v}\text{-}1)\cdot 10^3$	(2)				11.7	11.2	10.7	10.2	9.8	9.4
$\varepsilon_2 = (\alpha_{l\text{-}v}\text{-}1)\cdot 10^3$	(3)				112.3	104.7	97.7	91.1	85.0	79.3
Horita & Wesolowski (1994)										
$\varepsilon_{18} = (\alpha_{l\text{-}v}\text{-}1)\cdot 10^3$	(4)				11.8	11.3	10.7	10.2	9.8	9.3
$\varepsilon_2 = (\alpha_{l\text{-}v}\text{-}1)\cdot 10^3$	(5)				111.8	104.1	97.0	90.4	84.4	78.7
Merlivat & Nief (1967)										
$\varepsilon_2 = (\alpha_{l\text{-}v}\text{-}1)\cdot 10^3$	(6)			123.9	106.5	98.6				
$\varepsilon_2 = (\alpha_{s\text{-}v}\text{-}1)\cdot 10^3$	(7)	*198.4*	*173.1*	*151.1*	*131.8*					
Jakli & Staschewski (1977)										
$\varepsilon_{18} = (\alpha_{s\text{-}v}\text{-}1)\cdot 10^3$	(8)	*16.7*	*16.1*	*15.5*	*15.0*					
$\varepsilon_{18} = (\alpha_{l\text{-}v}\text{-}1)\cdot 10^3$	(9)				11.5	10.9	10.3	9.7	9.2	8.9

(1) $\ln \alpha_{18\text{-}O} = \ln (R_s / R_v) = 11.839/T - 28.224/1000$ $\quad 233 < T(K) < 273$

(2) $\ln \alpha_{18\text{-}O} = \ln (R_l / R_v) = 1137/T^2 - 0.4156/T - 2.0667/1000$ $\quad 273 < T(K) < 373$

(3) $\ln \alpha_D = \ln (R_l / R_v) = 24844/T^2 - 76.248/T + 52.612/1000$ $\quad 273 < T(K) < 373$

(4) $\ln \alpha_{18\text{-}O} = \ln (R_l / R_v) = 350410/T^3 - 1666.4/T^2 + 6.7123/T - 0.007685$ $\quad 273 < T(K) < 647$

(5) $\ln \alpha_D = \ln (R_l / R_v) = 1.1588\cdot T^3/10^9 - 1.6201\cdot T^2/10^6 + 0.79484\cdot T/10^3 - 0.16104 + 2999200 / T^3$ $\quad 273 < T(K) < 647$

(6) $\ln \alpha_D = \ln (R_l / R_v) = -0.1 + 15013/T^2$ $\quad 262.3 < T(K) < 278.5$

(7) $\ln \alpha_D = \ln (R_s / R_v) = -0.0945 + 16289/T^2$ $\quad 233 < T(K) < 273$

(8) $\ln \alpha_{18\text{-}O} = \ln (R_s / R_v) = 3.71/T^2 + 1.320/1000$ $\quad 223 < T(K) < 273$

(9) $\ln \alpha_{18\text{-}O} = \ln (R_l / R_v) = 9.275/T - 0.0225$ $\quad 273 < T(K) < 293$

$\ln \alpha_{18\text{-}O} = \ln (R_l / R_v) = = 5.869/T - 0.0108$ $\quad 293 < T(K) < 443$

4.2 Rayleigh Destillation

Assuming an isolated air mass, which is subjected to cooling and partial condensation and the subsequent removal of moisture by rain, the isotope variations in the course of this gradual rainout process can be described by a Rayleigh distillation equation (Dansgaard 1964)

$$\delta_v = (\delta_0+1)F^{(\alpha-1)} - 1 \tag{4.3}$$

$$\delta_l = \alpha_{l\text{-}v}\,(\delta_v+1) - 1 \tag{4.4}$$

where δ_0 is the initial isotopic composition of the vapour and F is the fraction of the initial moisture content remaining in the given air mass. Fig. 4.1(a) is a plot of $\delta^{18}O$ and δD of water vapour as a function of the fraction of vapour remaining with $\delta^{18}O_0$=–11‰ and δD_0=–78‰. Immediate removal of the liquid condensate without isotope exchange continuously depletes the remaining vapour in ^{18}O. The condensate that forms in equilibrium with this vapour also acquires lower and lower δ values as condensation proceeds. Thus, Rayleigh distillation results in much higher fractionation than processes that permit the two phases to equilibrate by exchange. The shift from F to condensation temperatures is easiest to calculate, at least under simplified conditions. The amount of water vapour remaining in an air mass under saturation conditions is a function of air temperature T and volume. Consequently, the $\delta - T$ relation depends on the way of cooling, Fig. 4.1(b). Isobaric cooling produces a steeper slope than moist-adiabatic cooling (lines A and B in Fig. 4.1b). The decrease of pressure of an air parcel upon uplifting is accompanied by a volume increase which results in a higher water vapour saturation mixing ratio.

Air mass cooling may proceed yet in another way. Turbulent mixing with cooler air mass results in fractionation which cannot be expressed by the Rayleigh condensation formula. Eriksson (1965) pointed out that $\alpha - 1$ in the Rayleigh formula should be replaced by $\sqrt{\alpha} - 1$ when considering an exponential decrease of specific humidity with distance and water vapour transport entirely by eddy diffusion. This implies that the isotopic fractionation is considerably less in eddy diffusion processes (lines C and D in Fig. 4.1b). An effect, which can be attributed to the horizontal or vertical mixing which acts to even out differences in the isotopic composition of water vapour in the atmosphere.

Plotting of δD versus $\delta^{18}O$ shows that the equilibrium condensation process results in a quasi linear relationship, Fig. 4.2. Adiabatic cooling produces steeper slopes than isobaric cooling in a δD–$\delta^{18}O$ diagram. The slope is also a function of the initial vapour

composition, the initial dew point, and the degree of cooling (Dansgaard 1964). Table 4.2 gives an overview on how these parameters change the slopes in a δD–$\delta^{18}O$ diagram. Precipitation in equilibrium with water vapour shows slightly steeper slopes due to the non-linear temperature dependence of the fractionation factors.

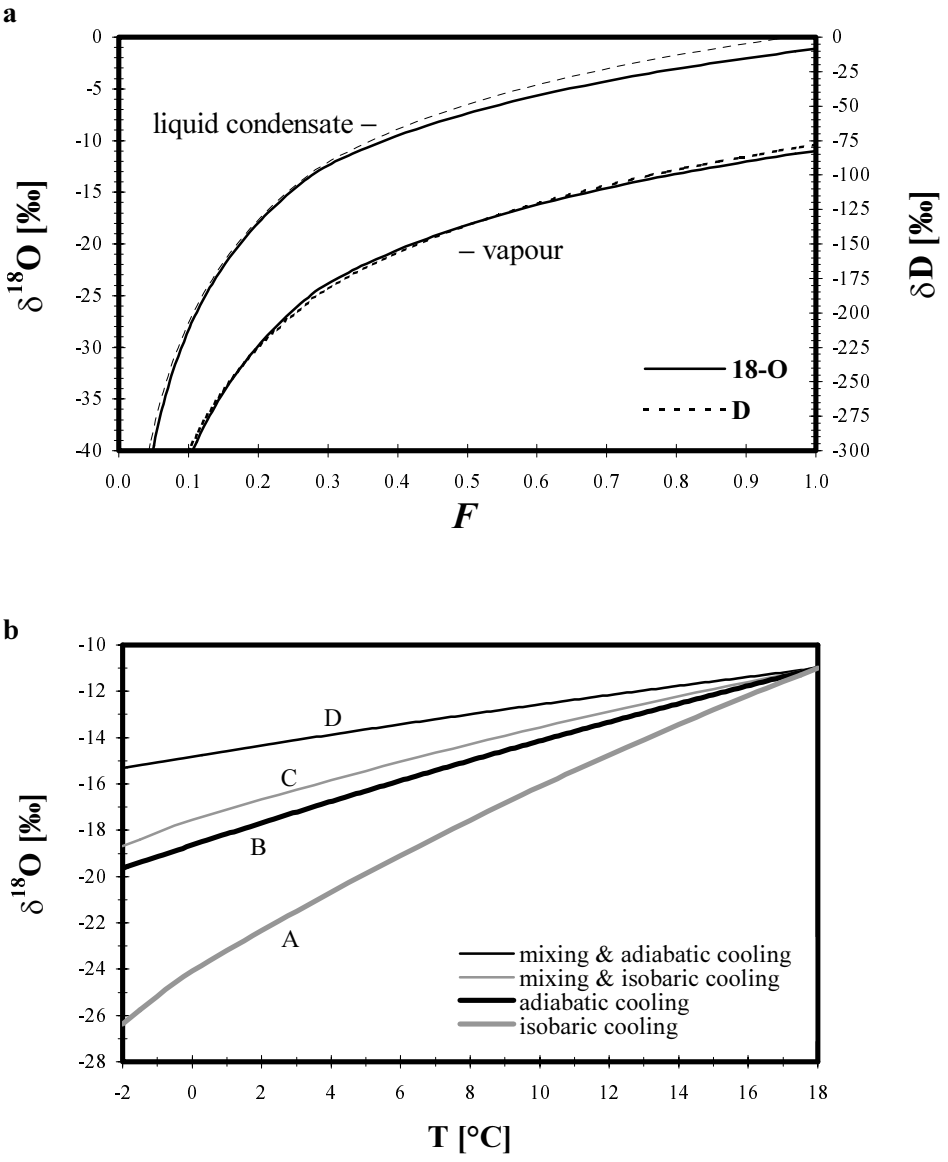

Fig. 4.1 (a) Isotopic fractionation due to condensation under Rayleigh conditions. $\delta^{18}O$ and δD of the remaining water vapour and of the newly formed liquid condensate as a function of the remaining fraction *F* of vapour. (b) $\delta^{18}O$ of the remaining water vapour as a function of temperature. A = isobaric cooling, B = adiabatic cooling, C = isobaric cooling including eddy diffusion, and D = adiabatic cooling including eddy diffusion.

Tabelle 4.2 Rayleigh model results: Slope of δD–$\delta^{18}O$ curves for water vapour for cooling to 273K. T_0 is the initial dew point temperature.

Type of cooling	$\delta^{18}O_0$[‰]	δD_0[‰]	slope of δD–$\delta^{18}O$ plot		
			T_0 = 298K	T_0 = 293K	T_0 = 288K
isobar	-15	-110	7.68	7.83	7.99
isobar	-11	-78	7.93	8.08	8.25
moist-adiabatic	-15	-110	7.93	8.02	8.14
moist-adiabatic	-11	-78	8.18	8.28	8.39

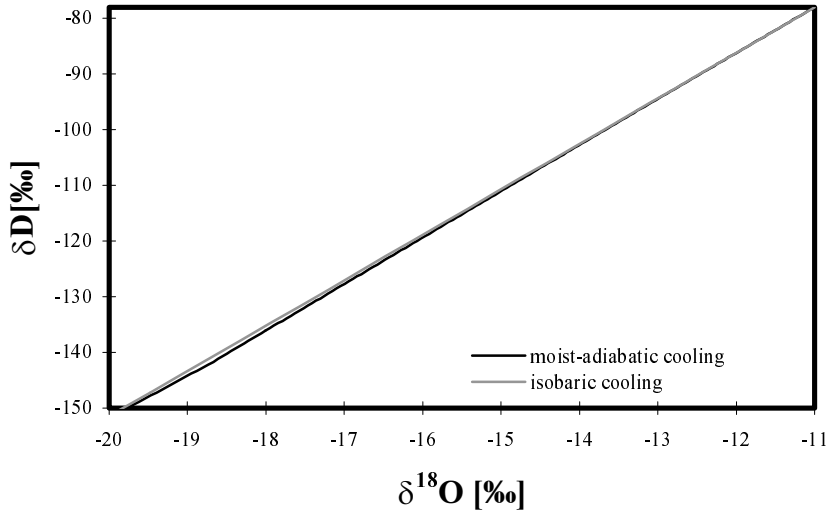

Fig. 4.2 Plot of calculated δD–$\delta^{18}O$ relations for water vapour. Rayleigh condensation starting at 18°C to 5°C for isobaric cooling and 18°C to –2°C for moist-adiabatic cooling.

On the basis of a large number of fresh water samples Craig (1961) showed that δD and $\delta^{18}O$ are linearly related and can be represented by the equation:

$$\delta D = 8 \cdot \delta^{18}O + 10 \qquad (4.5)$$

This linear relationship was later named the Global Meteoric Water Line (GMWL). The intercept depends on the evaporation mechanism. Sea water is generally isotopically well mixed with oxygen and hydrogen isotope compositions close to the standard V-SMOW (0±1‰). Diffusion of water molecules away from the liquid-air interface across the air boundary layer results in kinetic isotope fractionation.

Already in 1965, Craig & Gordon reported isotope compositions of water vapour over the North Pacific and the North Atlantic significantly more depleted in ^{18}O than water vapour in isotopic equilibrium with the sea surface.

The molecular diffusivities D of isotopically labelled water molecule species have the relation $D(H_2{}^{16}O) > D(HDO) > D(H_2{}^{18}O)$. The ratio of the molecular diffusion coefficients in air, of the pairs $H_2{}^{18}O/H_2{}^{16}O$ and $HDO/H_2{}^{16}O$ have been determined by Merlivat (1978) as 0.9723 and 0.9755, respectively. Note that the relative mass differences between the isotopic species of water cannot fully explain the observed molecular diffusion rates. The displacement of the center of gravity by isotopic substitution of the water molecule must be considered as well.

The deviation from equilibrium increases with the humidity deficit in the marine atmosphere. In order to simplify terminology, Dansgaard (1964) introduced the deuterium excess for precipitation, defined as:

$$d_{prec} = \delta D - 8.00\ \delta^{18}O \tag{4.6}$$

The deuterium excess has become a valuable tool to derive information on source conditions (e.g. relative humidity, magnitude of the diffusive sublayer) from isotope data which are otherwise not accessible.

The empirical factor of 8.00 in equation (4.6) is valid only for precipitation and freshwater. Previous studies revealed that the local meteoric water lines (LMWLs) of water vapour and precipitation have slightly different slopes in a $\delta D - \delta^{18}O$ plot (Jacob & Sonntag 1991, Schoch-Fischer *et al.* 1984). The LMWL for precipitation from 1981 to 1988 in Heidelberg has a slope of 8.06, while the slope of water vapour over the same time span is only 7.71. The average slope of Central European precipitation has a slope even closer to the global mean with 7.99.

The different slopes for vapour and precipitation is due to the temperature dependent isotope fractionation factors for evaporation of water. Rayleigh condensation yields slopes between 7.68 and 7.83 for the residual vapour under isobaric cooling with an initial dew point temperature between 25°C and 20°C, respectively (Table 4.2). Agemar et al. (2001) introduced a new deuterium excess parameter specifically for water vapour. The deuterium excess for water vapour is defined in the same way as the deuterium excess for precipitation and freshwater but the factor 8.00 is replaced by 7.75 according to theoretical considerations and field measurements:

$$d_{vap} = \delta D - 7.75\ \delta^{18}O \tag{4.7}$$

Water vapour samples collected at altitudes up to 5 km in the vicinity of Heidelberg indicated a significantly steeper slope, $\Delta\delta D / \Delta\delta^{18}O = 8.3$ (Taylor 1968) than our samples collected near the ground over two decades, $\Delta\delta D / \Delta\ \delta^{18}O = 7.8$. The higher slope encountered in the free troposphere can be explained by an adiabatic cooling

history. The d_{vap}-parameter (in eqaution 4.7) only applies to vapour samples with mostly isobaric cooling histories.

4.3 Evaporation from Open Surface Waters

When the air is not saturated with water vapour, a net evaporation flux occurs. If evaporation is at steady state, the evaporation flux E is constant over the vertical z-axis. The isotopic exchange effects in the evaporation of water can be calculated by dividing the constant flux layer into a layer just above the air-water interface where mass transport occurs by molecular diffusion and an overlying fully turbulent layer (Craig & Gordon 1965, Merlivat & Contiac 1975). This approach has proved to be in excellent agreement with various air-water tunnel experiments (Merlivat 1978).

The first mathematical expression for the isotopic composition of E were presented by Craig and Gordon in 1965. Their flux equations are based on the linear resistance model of Rideal and Langmuir in which the fluxes are related to the concentrations at the layer boundaries and the resistance to transport across the layer.

The flux equations of Merlivat & Contiac (1975) are virtually identical with the expressions of Craig & Gordon, but simpler in type. They are based on universally accepted evaporation theories. The major difference to Craig & Gordon is that Merlivat & Contiac do not treat diffusive fractionation in the liquid phase. Thus, a slight enrichment in the liquid has to be considered when applying their equations. The air-water interface is generally characterised by isotopic equilibrium ($R_s = R_l / \alpha$) and water vapour saturation.

$$E = \Gamma\rho\,(q_s - q) \tag{4.8}$$

$$E_i = \Gamma\rho\,(q_{s\,i} - q_i) \tag{4.9}$$

with $\frac{q_{si}}{q_s} = R_s = \alpha \cdot R_l$, and $\frac{q_i}{q} = R_v$ (4.10)

where ρ is the air densitiy, q_s is the saturated specific humidity, q the specific humidity at the height z, and Γ is the profile coefficient at z. The profile coefficient Γ has been introduced by Merlivat & Contiac (1975) in order to use the flux equations for various evaporation models. A general expression for Γ is

$$\Gamma = \frac{u*}{\rho_M + \rho_T} \tag{4.11}$$

where ρ_M and ρ_T are the molecular and turbulent resistances, respectively. The friction velocity $u*$ is related to surface roughness length z_0 and wind velocity u at z (Roedel 1994, p. 291):

$$u* = \frac{\kappa}{u \cdot \ln \frac{z}{z_0}} \tag{4.12}$$

where κ is the von Karman constant; its experimental value is 0.4.

Brutsaert (1965, 1975) considers evaporation as a molecular diffusion process into Kolmogorov-scale eddies which are renewed intermittently after random times of contact with the evaporating surface. This transient eddy model of Brutsaert gives the following two expressions for ρ_T / ρ_M :

$$\frac{\rho_T}{\rho_M} = \frac{\frac{1}{\kappa}\ln\frac{u*z}{30}}{13.6 \cdot Sc^{2/3}} \qquad \text{n} = {}^2/_3 \text{ for smooth surface regimes } (R_e<0.13) \text{ and} \tag{4.13}$$

$$\frac{\rho_T}{\rho_M} = \frac{\frac{1}{\kappa}\ln\frac{z}{z_0} - 5}{7.3R_e \cdot Sc^{1/2}} \qquad \text{n} = ½ \text{ for rough surface regimes } (R_e>2). \tag{4.14}$$

The term *Sc* is the Schmidt number, defined as $Sc=\nu/D$ with ν as the kinematic air viscosity and D the molecular diffusivity in air; resulting in Sc = 0.62. For a smooth interface, the Brutsaert's evaporation model shows that $\rho_M \propto D^{-2/3}$ and accordingly $\rho_M / \rho_{M,i} = (D_i/D)^{2/3}$. For a rough surface regime $\rho_M / \rho_{M,i} = (D_i/D)^{½}$ is more appropriate. Now, the isotope composition of the evaporation flux can be obtained from (4.8) and (4.9)

$$R_E = \frac{E_i}{E} = \frac{\Gamma_i (q_{si} - q_i)}{\Gamma (q_s - q)} \tag{4.15}$$

A δ expression for the evaporation flux can be obtained from (2.1), (3.9), and (3.14):

$$1+\delta_E = (1-k)\frac{\delta_l \alpha^{-1} - h(1+\delta_v)}{1-h} \tag{3.15}$$

with $h = q/q_s$ and 1-k = Γ_i/Γ. All non-equilibrium effects are included in the parameter k, attributed to the diffusion of vapour from the air-water interface into the free atmosphere. Water surfaces are generally smooth with roughness lengths between 10^{-5} and 10^{-4}m (Roedel 1994 p. 293, Barry & Chorley 1995 p.101). In this case, k is fairly constant for wind speeds u > 3 m/s. The values for k plotted in Fig. 4.3 have been calculated for an evaporation temperature of 25°C and a mean roughness length of $5 \cdot 10^{-5}$m.

Equation (4.16) clearly shows that the isotopic composition of the evaporation flux is very sensitive to changes in the relative humidity, the isotopic composition of atmospheric moisture, and the temperature of the inteface.

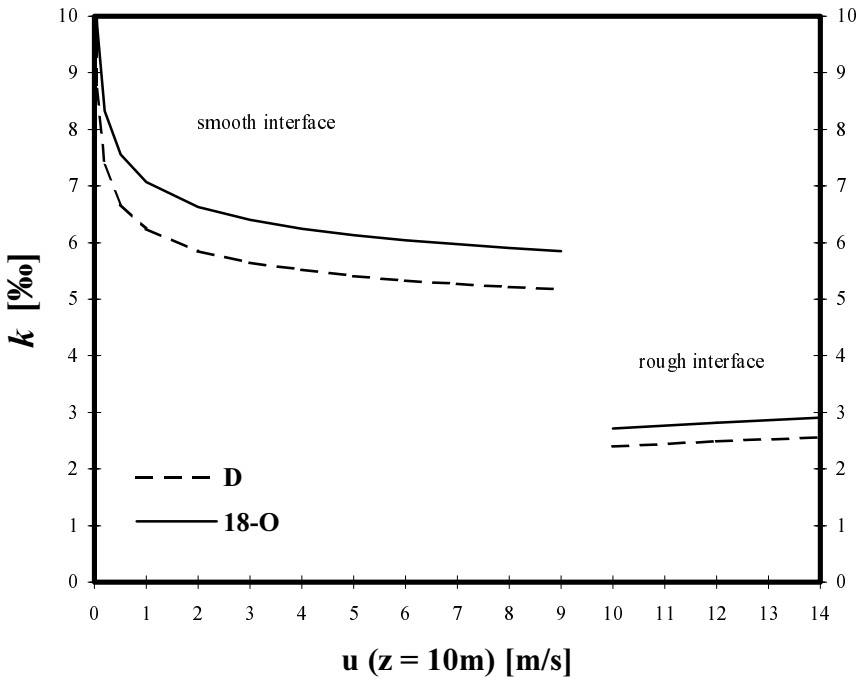

Fig. 4.3 The kinetic fraction parameter k as a function of the mean wind speed at z = 10 m and with a surface roughness of $5 \cdot 10^{-5}$ m.

5

The Stable Isotope Content of Water Vapour and Precipitation

The seasonal variation of deuterium excess in atmospheric water vapour can be explained by using 5-day backward trajectories to detect the imprint of local conditions at source regions. Although the subtropical Atlantic is an important moisture source for the northern westwind belt, seasonal variation of deuterium excess in Europe is rather controlled by regional evaporation.
The relationship between long-term changes of the isotopic composition of atmospheric water vapour and surface air temperature is most useful for the calibration of a paleo-isotope-thermometer. This study shows that the $\delta - T$ relations of annual means of the isotopic composition of water vapour at Heidelberg and Central European precipitation are nearly identical. The δ–T slope of the seasonal variations is high in winter but low in summer. The flat δ–T relation in summer is mainly due to the positive sea-land temperature gradient, reducing the effect of Rayleigh distillation and the continuous recharge of water vapour transpired by plants.

5.1 Description of the Data Set

5.1.1 18-year Record of Stable Isotopes in Water Vapour

The water vapour collection at the Institut für Umweltphysik (IUP) in Heidelberg provides isotopic data on atmospheric water vapour for the years 1981 to 2000. The sampling site is located on the east side of the upper Rhine Valley at 49°25’ N and 8°41’ E, 125 m above sea level. The air inlet is ~15 m above ground. The S-N trending Rhine valley and the W-E trending Neckar valley force local winds which superimpose synoptic-scale wind patterns at Heidelberg.

The sampling device for continuous vapour collection (Schoch-Fischer et al., 1984) has not been changed since 1981. However, sampling time varied between one and three days. Water vapour is collected in a cold trap (-48 to -44°C) over 1 to 3 days at flow rates between 10 and 60 L STP per hour which results, with the sampling times above, in 600 to 2000 L processed air. Altogether, 2753 high-quality water vapour samples have been collected.

The samples were analysed mass-spectrometrically using a modified H_2O-CO_2 equilibration technique (see section 3.1) for $\delta^{18}O$ and reduction over hot zinc (Tanweer et al. 1988) and – more recently – hot chromium (Gehre *et al.* 1996) for δD. The data are corrected for non-quantitative sampling according to formula 3.7. The total error of analysis including correction has been determined experimentally to be ±3.6‰ for δD and ±0.3‰ for $\delta^{18}O$ (±2.8‰ for δD and ±1.1‰ for $\delta^{18}O$, Schoch-Fischer *et al.* 1984).

During the first years (1981 to 1982), the radioisotope ratio T/H was also measured by a low-level proportional counter. The water vapour content of the air was derived from the sampled quantity of moisture related to the air mass which has passed through the sampling device.

5.1.2 Selected Data from the GNIP-Database (IAEA/WMO)

The data of our 18-year atmospheric water vapour record have also been compared with the averaged isotopic composition of precipitation at 15 sites in Germany, one in Vienna (Austria) and one in Cracow (Poland) which were extracted from the IAEA/WMO database GNIP (Global Network for Isotopes in Precipitation) for the period from January 1981 to December 1995.

5.1.3 Back Trajectories

To relate the actual isotope data to the moisture sources and sinks of the air mass along its pathway over ocean and land areas, 5-day isobaric (925 hPa) back trajectories calculated by Atmospheric Environment Service (AES, Toronto, Canada) were used. The model LRTAP (= Long Range Transport of Air Pollutants), described by *Olson et al.* (1978) uses the meteorological analysis from the Canadian Meteorological Centre with a 381 km horizontal grid resolution at five pressure levels. The trajectories were retrieved every six hours (0, 6, 12, 18h) for the period from July 1992 to December 1995. Air mass positions are calculated at six hour intervals. Generally, one water vapour sample is collected over a time span pertaining to 8 – 12 trajectories.

Additionally, 3-D trajectories have been obtained from Deutscher Wetterdienst for August 1994 for 9 pressure levels at Heidelberg (surface pressure minus 6 hPa, 975hPa, 950hPa, 850hPa, 800hPa, 750hPa, 700hPa, 600hPa and 500hPa). A comparison reveals marked discrepancies between 3-D and isobaric trajectories. However, for the purpose of this study, even isobaric trajectories suffice for the determination of water vapour source regions.

5.1.4 Meteorological Data

Unfortunately, daily weather data of the Institut für Umweltphysik (IUP) could not be used since the record does not cover the full time span of this study. Furthermore, IUP air temperatures are on average 1K lower at 25°C and 0.4K higher at 0°C than those of the Deutscher Wetterdienst (DWD) in Offenbach (Germany) or the National Climatic Data Center (NCDC) in Asheville, NC (U.S.A.). These deviations are likely to be due to the roof location of the IUP weather station.

Therefore, daily weather data have been supplied by the DWD for the period 1st January 1980 to 30th October 1997. The weather station ‚Heidelberg' is located 1km east of the sampling site at 49°25' N and 8°40' E at an elevation of 110 m. The NCDC-data have been downloaded from the IRI/LDEO Climate Data Library (http://ingrid.ldeo.columbia.edu/) and converted from Fahrenheit into degree Celsius.

In addition, the NCDC data covers the period from 1 May 1997 to 31 December 1999 for the weather station ‚Heidelberg (USA-AF)' which is located 49°24' N and 8°39' E at an elevation of 109 m (approximately 3km southeast of the sampling site). Although the two datasets are derived from two different weather stations, the data coincide remarkably well. The mean air temperature 2 m above ground is on the average only 0.09°C higher at the American weather station compared to the German weather station. Therefore, NCDC data have been used from 31 October to 31 December 1999.

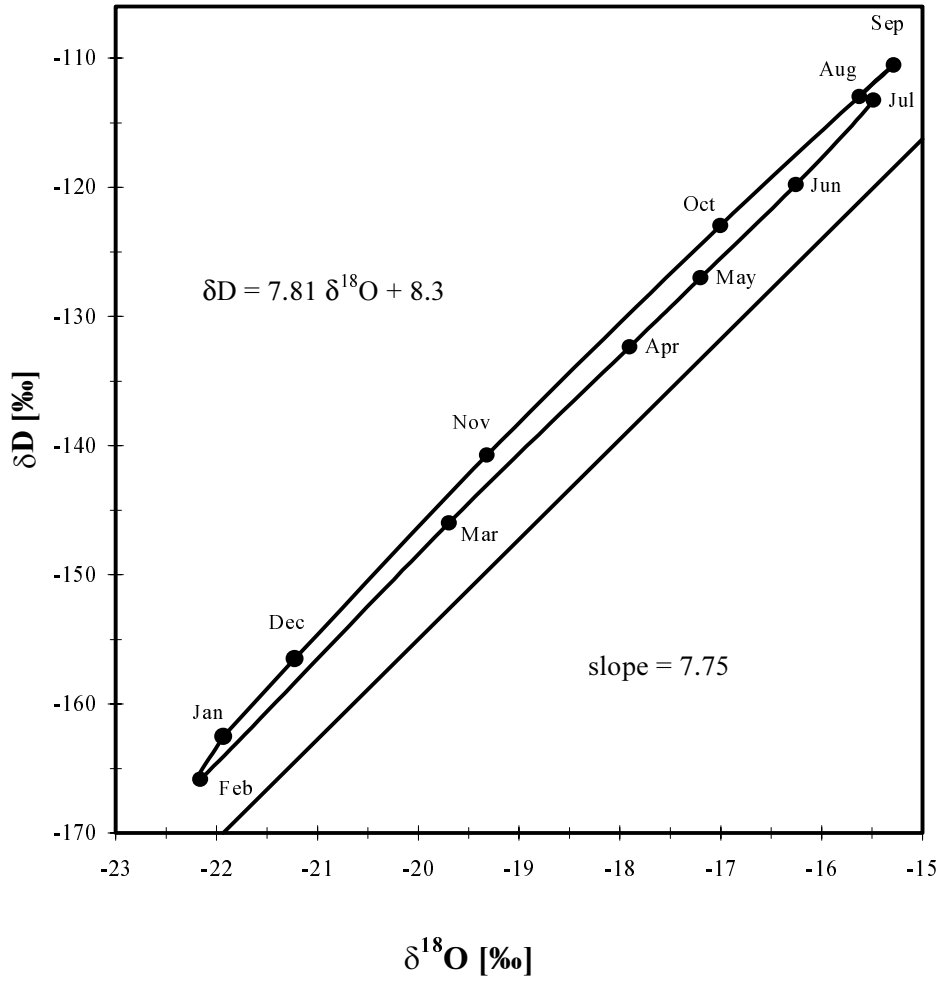

Fig. 5.1 The LMWL (local meteoric water line for water vapour at Heidelberg has been calculated from monthly means. The bold line is the reference for zero deuterium excess (d_{vap} = 0). The hysteresis loop is the result of variable deuterium excess.

5.2 The δD – δ^{18}O Relation

Table 5.1 gives an overview on the number of vapour samples and monthly mean δD and δ^{18}O values. A plot of δD versus δ^{18}O in Fig. 5.1 displays the LMWL of water vapour at Heidelberg for unweighed monthly averages. The hysteresis loop reveals that d_{vap} varies with a significant time lag (2 to 3 months) behind δ's. This is confirmed in Fig. 5.2 which shows that deuterium excess d_{vap} follows a seasonal cycle with maximum values from August to November whereas δD and δ^{18}O minimize in winter. Note that the seasonal variation of d_{vap} is very similar in phase and amplitude to the average d_{prec} for Central Europe.

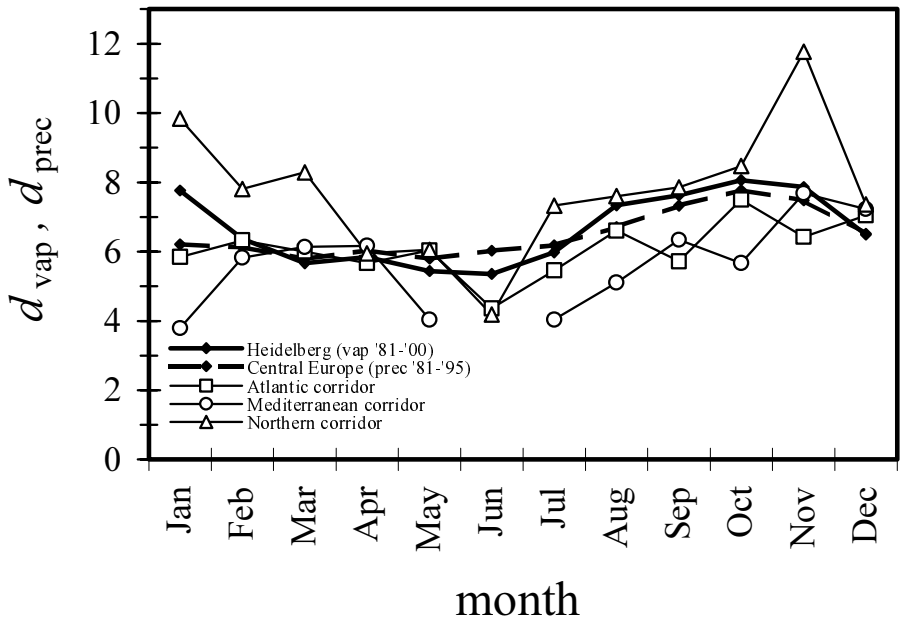

Fig. 5.2 Seasonal variations of deuterium excess in vapour at Heidelberg and in Central European precipitation show identical phase and amplitude (bold lines). Back trajectories have been used to identify different corridors. Because trajectories were available for three and a half years, only, d_{vap} values associated to a corridor have been normalised to the d_{vap} values for Heidelberg (1981-2000).

The seasonality of the Central European deuterium excess differs from the typical deuterium excess patterns observed at many other GNIP stations. Precipitation within the North Atlantic westwind belt shows high d_{vap}-values with a seasonal maximum in January. The IAEA/GNIP survey (1999) reports monthly mean d_{prec}-values of up to 31.8‰ for winter precipitation at the Goose Bay station on Newfoundland (53.3°N, 60.4°W). This is due to dry continental air masses advected over warm Atlantic sea water. Another example is Tokyo which has a distinct maximum in deuterium excess in January, too, because westerly circulation in winter conveys cold continental air masses over the Japan Sea and the China Sea where rapid evaporation with enhanced kinetic fractionation takes place. A similar situation is observed for the Azores which receives precipitation from the tropical Atlantic in summer, whereas in winter easterly circulation dominates, advecting dry air masses from the Sahara over the East Atlantic to the islands. Very high d_{prec}-values are also found at the Mediterranean where dry winds from the Sahara blow over the sea (Gat et al. 1996, Rindsberger et al. 1983). However, Heidelberg rarely receives air masses from the Mediterranean (nor from the Black Sea which is also known for high d_{prec}-values). The Alps are obviously an effective shield against meridional moisture transport from the south. The northern westwind belt is the dominant conveyer of moisture for the European continent.

Using backward air mass trajectories, we found that days with extremely high d_{prec} values in autumn are caused by cold polar or continental air masses which cross the North Sea or the Baltic Sea, Fig. 5.3(a-f). The back trajectories can be grouped into three corridors, namely the Atlantic corridor, the northern corridor and the Mediterranean corridor. Extending the view to whole months, we observe that deuterium excess in air masses from the northern corridor is in most cases higher than in air masses from the Atlantic or the Mediterranean corridor. The difference in deuterium excess is most pronounced in autumn and winter, Fig. 5.2.

Polar and Siberian air masses belong to the northern corridor which encompasses 33% of all trajectories. The mean d_{vap} value (for the period 7/1992 to 12/1995) is 11.0‰. Trajectories from the Mediterranean corridor contribute only 17% of all trajectories. The mean d_{vap} value is 8.9‰. Air masses from the Atlantic corridor also show rather low d_{vap} values (= 8.8‰) for the same time period. Due to the dominant westerly circulation, 51% of the trajectories come from this direction. However, the seasonal phase of d_{prec} at Atlantic stations is markedly different from European stations.

The large temperature difference between continental air and the sea in autumn and winter results in very low humidity which results in rapid evaporation. This is reflected in the average evaporation rates over the North Sea with 25 mm/month in spring and 75 mm/month in autumn. However, depending on the daily weather situation, evaporation rates up to 15 mm/day are possible. Thus, even short passages over the sea may change the deuterium excess significantly. Fig. 5.3(a), for instance, shows Siberian air masses advected over the Baltic Sea. The original d_{vap}-value can be estimated from IAEA/WMO (1999) precipitation data to be +10‰. Thus, d_{vap} has been doubled by evaporation over the Baltic Sea.

On the other hand, Fig. 5.3(e) shows air masses of westerly origin with very low deuterium excess although strong evaporation (up to 300 mm/month) at the lee-side of the North American continent in winter produces extremely high d_{vap}-values. The low deuterium excess at the end-point in Heidelberg can indeed be explained by isotopic exchange between atmospheric moisture and sea surface water. The isotopic exchange between the ocean and water vapour in the atmosphere is 40 times faster than evaporation. Thus, deuterium excess in water vapour will adjust to changing humidity and sea surface temperatures within three days. This point will be discussed in further detail in Chapter 6 when computer model results will be used to illustrate the isotopic exchange between surface water and water vapour.

Table 5.1 Overview on monthly mean isotopic composition of atmospheric water vapour, absolute humidity and total number of all samples for each month.

		unweighted means			weighted means			abs. hum.
month	**samples**	**δ^2H [‰]**	**δ^{18}O [‰]**	***d* [‰]**	**δ^2H [‰]**	**δ^{18}O [‰]**	***d* [‰]**	**[g/m^3]**
Jan	254	-160.2	-21.6	7.5	-154.6	-20.9	7.0	4.74
Feb	243	-165.1	-22.0	5.4	-155.2	-20.8	6.4	4.57
Mar	262	-144.3	-19.5	7.0	-140.1	-18.9	6.5	5.44
Apr	216	-140.8	-19.1	6.9	-138.7	-18.8	7.3	6.03
May	229	-127.7	-17.3	6.4	-126.3	-17.1	6.3	8.39
Jun	179	-119.3	-16.2	6.0	-118.7	-16.1	6.0	10.86
Jul	235	-113.4	-15.5	6.7	-111.7	-15.3	6.6	11.74
Aug	230	-113.7	-15.7	7.9	-111.7	-15.4	7.9	11.53
Sep	224	-116.6	-16.1	8.2	-115.6	-16.0	8.1	10.67
Oct	252	-129.3	-17.9	9.2	-131.8	-18.2	9.3	8.26
Nov	233	-147.5	-20.3	9.6	-142.7	-19.6	8.9	6.21
Dec	196	-156.3	-21.2	7.8	-152.8	-20.7	7.7	5.29
	Σ=2753	Ø = -136.2	Ø = -18.5	Ø = 7.4	Ø = -133.3	Ø = -18.1	Ø = 7.3	Ø = 7.8

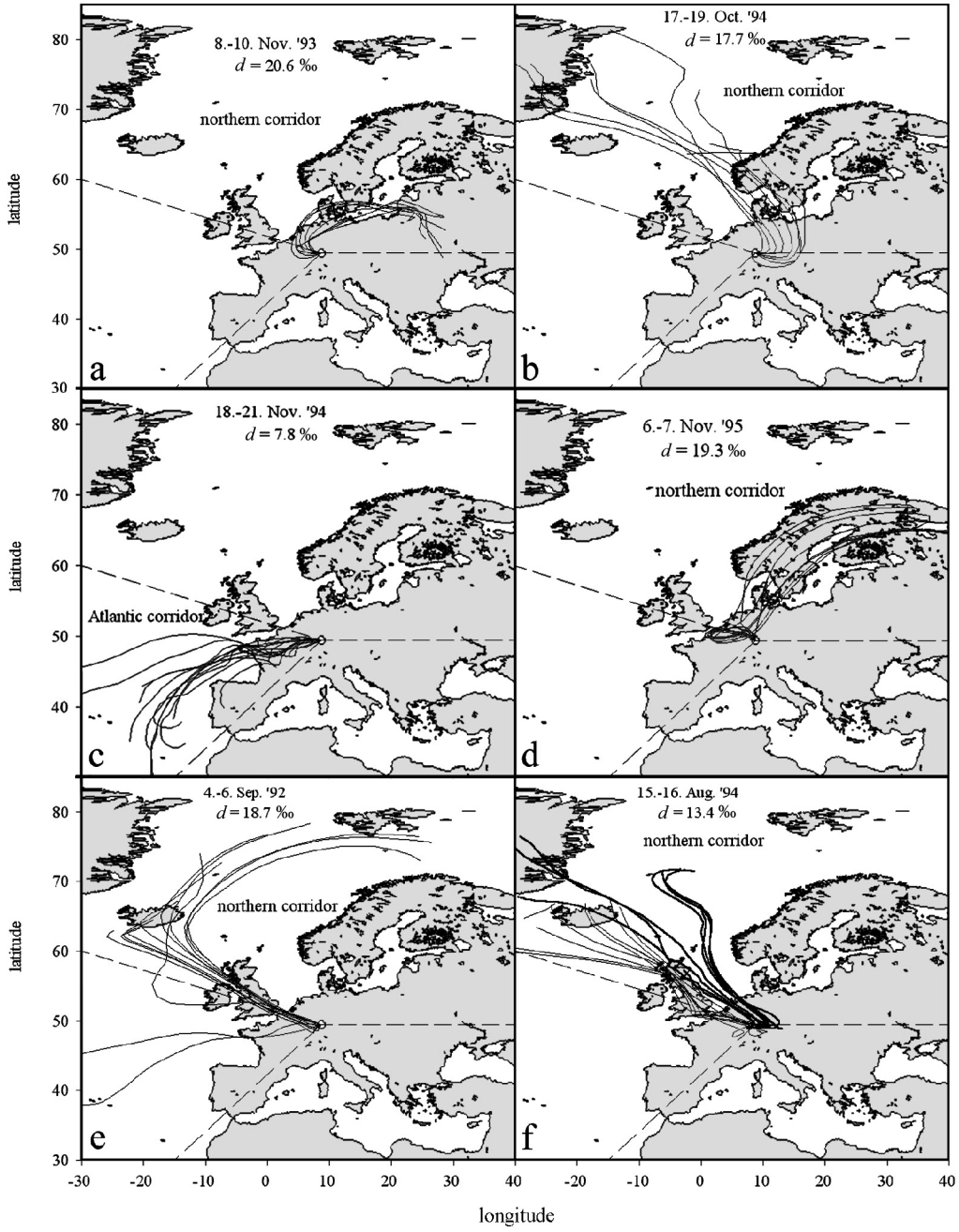

Fig. 5.3 Five-day-back-trajectories isobaric at 925 hPa: (a) A low pressure cell over East-Europe on 8th-10th November '93 conveys cold and dry continental air over the Baltic Sea to Heidelberg. The deuterium excess in water vapour is very high due to rapid evaporation over the open water surface. (b) Cold and dry Arctic air on 17th-19th October '94 takes up moisture from the North Sea and raises its d_{vap} to 17.7‰. (c) Warm south-easterly circulation over Europe brings air with a low d_{vap} of only 7.8‰ on 18th-21st November '94. (d) Cold air from Finland is convected over the Baltic Sea and raises the d_{vap} to 19.3‰ on 6th-7th November '95. (e) Arctic air masses move from Iceland over Great Britain and the Channel to Heidelberg on 4th-6th September '92. A d_{vap} of 18.7‰ indicates rapid evaporation over the North Sea and the Channel. (f) Similar situation as in (e) but on 15th-16th August 1994. Bold lines represent 3D-four-day-back trajectories (950hPa at Heidelberg).

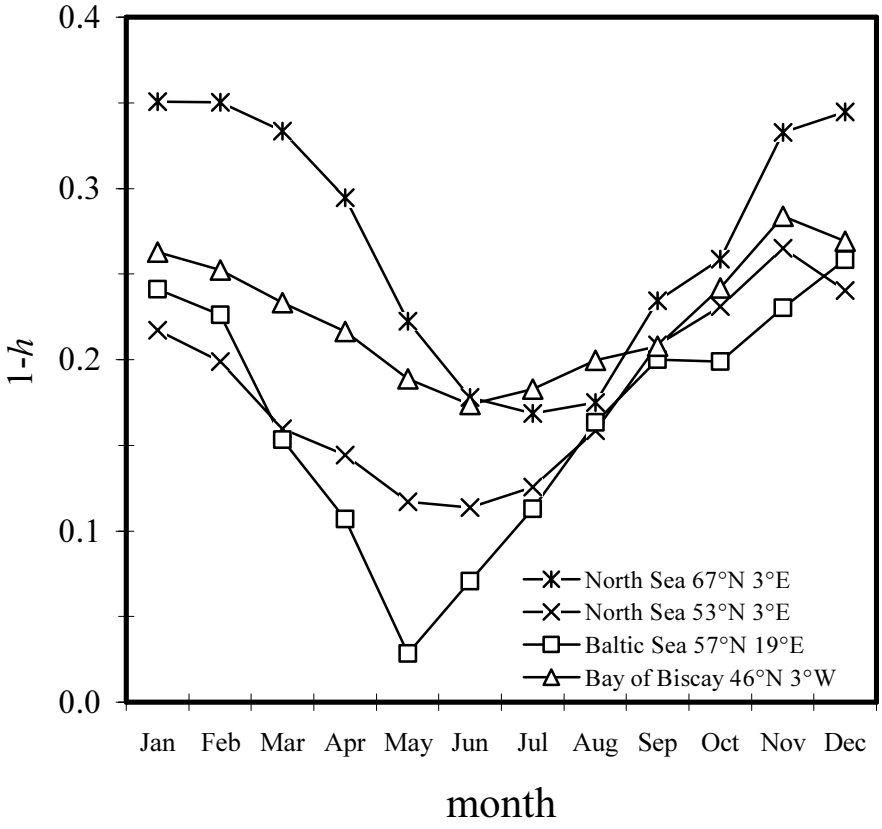

Fig. 5.4 Seasonal variations of the humidity deficit relative to sea surface temperature over the North Sea. The humidity deficit decreases from north to south, but the timing of the maximum humidity deficit also changes from November to January. (Data from Oberhuber 1988)

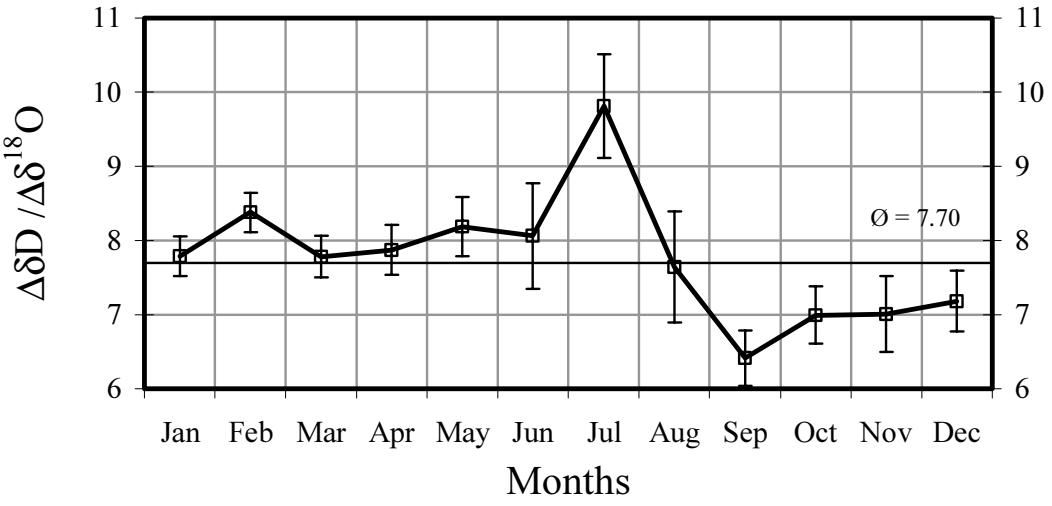

Fig 5.5 Monthly climatology of the slopes of water vapour MWLs at Heidelberg.

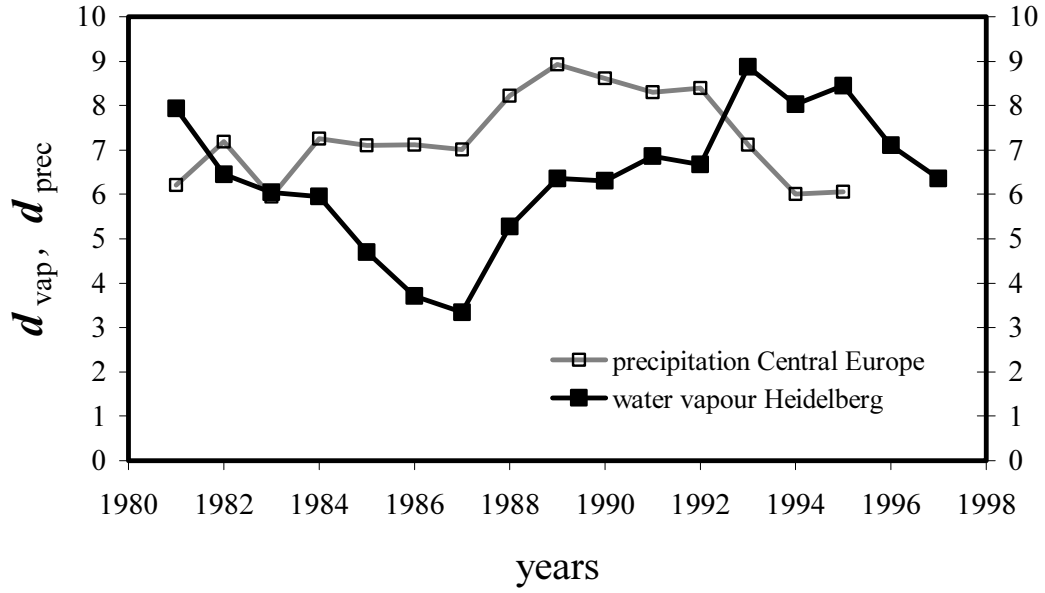

Fig 5.6 Annual variations of d_{vap} at Heidelberg.

The unusual δ-*d* phase relation in European water vapour and precipitation can be explained with the meteorological conditions in the vicinity of the European continent. The relative humidity data shown in Fig. 5.4 are calculated relative to sea surface temperature rather than air temperature because of the thin (<0.1mm) laminar-viscose layer at the air-sea interface. Craig & Gordon (1965) confirm that humidity and isotopic composition of marine air moisture correlate fairly well when humidity is reduced to the sea surface temperature. A correlation between Central European deuterium excess and humidity deficit can be found for the Bay of Biscay and the North Sea. The maximum humidity deficit over the southern North Sea and the Bay of Biscay occurs in November, whereas at higher latitudes, the maximum humidity deficit is reached in January – paralleling the deuterium excess in precipitation on Iceland. A comparison of air masses reveals that northerly circulation over the North Sea and the Baltic Sea enhances annual deuterium excess by 0.7‰ on the average.

Furthermore, it must be considered that the influence of the humidity deficit over the sea on deuterium excess in continental water vapour and precipitation also depends on the prevailing winds. The advection of polar and Siberian air masses over the warm surface waters of the North Sea and the Baltic Sea in autumn results in enhanced humidity deficits. This explains why polar and Siberian air masses show extremely high d_{vap} values in autumn and winter. During westerly circulation, evaporation over the North Sea and the Baltic Sea do not contribute to Central European atmospheric moisture. In this case, evaporation over the Bay of Biscay controls deuterium excess in atmospheric moisture over Europe. The seasonal phase of the humidity deficit and, in

turn, the deuterium excess is also controlled by the Gulf Stream which is responsible for warm sea surface waters in Europe over an extended period of time in the year.

Studies on high-latitude precipitation often argue that distant vapour sources are responsible for phase and amplitude of deuterium excess (e.g. Ciais et al. 1995, Johnson et al. 1989). These studies, however, do not treat regional isotopic exchange between atmospheric moisture and surface water which is important to the evolution of deuterium excess in atmospheric water vapour.

The careful investigation of backward trajectories over Europe reveals that the origin of deuterium excess must be regional. For Europe, the Gulf Stream plays a crucial role in establishing the δ–d phase relation because sea surface temperatures affect the humidity deficit in the air.

The regional roots of deuterium excess are also evident in the slope of the $\delta D - \delta^{18}O$ relation for individual months, Fig. 5.5. The lowest slopes are found from September to December. The low slopes indicate that months with moisture more depleted in heavy isotopes have higher d_{vap} values because high d values and low δ values lowers the slope of the $\delta D - \delta^{18}O$ relation. This is what can be expected because polar and cold continental air masses show the highest d_{vap} values in autumn in Heidelberg. Atmospheric moisture of polar or cold continental air masses is generally very depleted in heavy isotopes and the uptake of water vapour from the oceans involves kinetic fractionation resulting in higher d_{vap} values. The very steep slope for July in Fig. 5.5 may surprise but can be explained by partial evaporation of rain drops in unsaturated air beneath the cloud base (Stewart 1975). This process increases the d_{vap} and enriches the vapour in heavy isotopes because precipitation is generally heavier than atmospheric moisture. However, this phenomenon is restricted to hot summer months with frequent precipitation events; it does not alter the principal behaviour of deuterium excess.

Fig. 5.6 shows the record of the annual mean deuterium excess in vapour and in precipitation over two decades. The eighties have significantly lower d_{vap} values than the nineties. The annual mean d_{prec} values show a different trend which may be due to the sporadic nature of rainfalls.

5.3 Short-term Variations

Diurnal variations of humidity, air temperature and plant activity may also affect the isotopic composition of atmospheric moisture, as has been shown by experiment (Bariac et al. 1990; Yakir et al. 1994; Wang & Yakir 2000). At steady state, the isotopic composition of water vapour transpired by plants is the same as in the soil layers

supplying water to the roots. There is no fractionation during water uptake by the roots. Soil water is generally enriched when compared with regional water vapour.

The influence of the vegetation on atmospheric moisture is most pronounced when in summer a high pressure cell over central Europe reduces advectivion. This has been the case on 27th to 29th August 2000, the time of an experiment which was conducted to estimate the temporal evolution of the isotopic composition of water vapour, Fig. 5.7. The water vapour released by plants changes the isotopic composition of atmospheric moisture predominantly during daytime when relative humidity is low and transpiration reaches its maximum. Fig. 5.7 shows that $\delta^{18}O$ of water vapour at noon is approximately 2‰ higher than in the early morning.

The enrichment in heavy isotopes in atmospheric moisture during daytime can be used to assess the contribution of local evapotranspiration. The water vapour released into the atmosphere has a $\delta^{18}O$ value of approximately -6‰ which is 8‰ higher than the lowest $\delta^{18}O_{vap}$ in the course of a day. This implies that the contribution of recently transpired plant water (within the last 12 hours) in the sample with maximum ^{18}O content is approximately 25%. The overall contribution of transpired plant water within one sample is of course higher, due to continuous recharge by plant transpiration over several days before any airmass reaches Heidelberg.

Note that d_{vap} shows similar diurnal variations as δ. However, the deuterium excess in soil water does not differ very much from d_{vap} in the atmosphere. The increase in d_{vap} during mid-day can be related to the drop in relative humidity and the time needed by plants to response to the changed hydro-meteorological conditions.

However, variations in the local weather regime may affect the isotopic signal in atmospheric moisture much more than diurnal variations of air temperature and plant activity. Fig. 5.8 shows a 5-day record of δD, d_{vap} and air temperature in February 2000. The record exhibits a large drop in δD after 18.00h on February the 10th which coincides with a period of heavy rainfall from 19.30h to 2.30h of the next day. The weather station on the roof of the IUP recorded 14.6 mm of precipitation within 7 hours and strong winds from the south turning to the west with up to 68 km/h velocity. Relative humidity increased from 50% to nearly 90%.

The plot of 3-D back trajectories (Fig. 5.9) reveals strong cyclonic lofting of moist polar air masses in a low pressure system. The uplift of warm, less-dense air from the west triggers 'cyclonic type' precipitation. The very low δ-values can be attributed to the "amount effect": moist-adiabatic uplifting results in deep cooling. As cooling proceeds, δ-values of the condensate decrease, whereas the total amount of precipitation increases. The fractionation by isotopic exchange between falling drops and the environmental vapour also lowers the δ-value of the vapour because in heavy rain the vapour composition is largely determined by the liquid phase. Thus, the sharp decrease of δD in vapour in Fig. 5.8 is due to the formation of precipitation at high

altitudes and deep cooling. The 'amount effect', however, is typically observed in heavy thunderstorms in summer and not a general feature of winter rain fall at Heidelberg. Usually, winter precipitation is of an orographic/cyclonic origin and forms at lower altitudes.

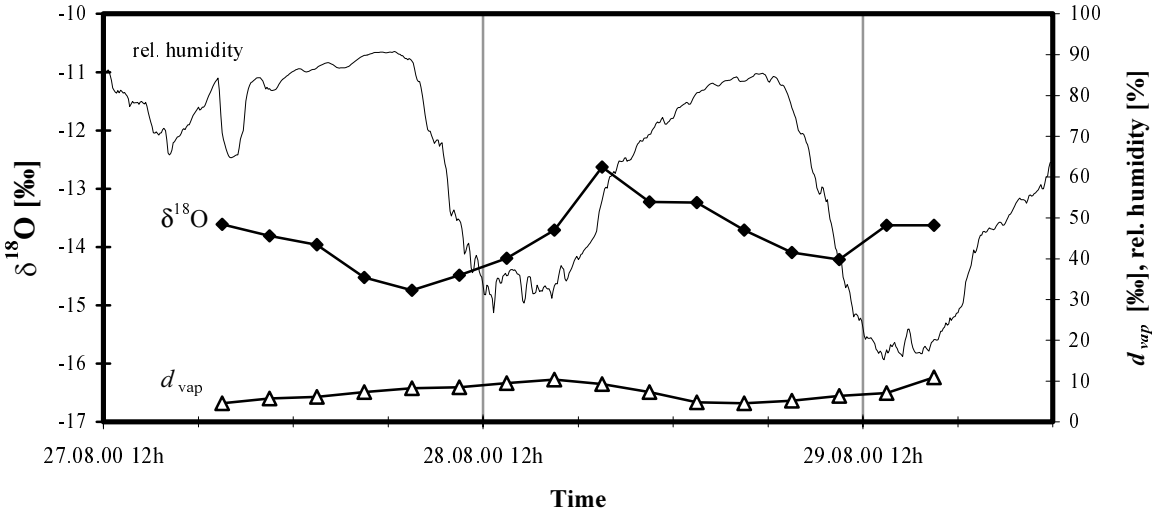

Fig 5.7 Fluctuations of $\delta^{18}O$, d_{vap}, and relative humidity over 5 days in August.

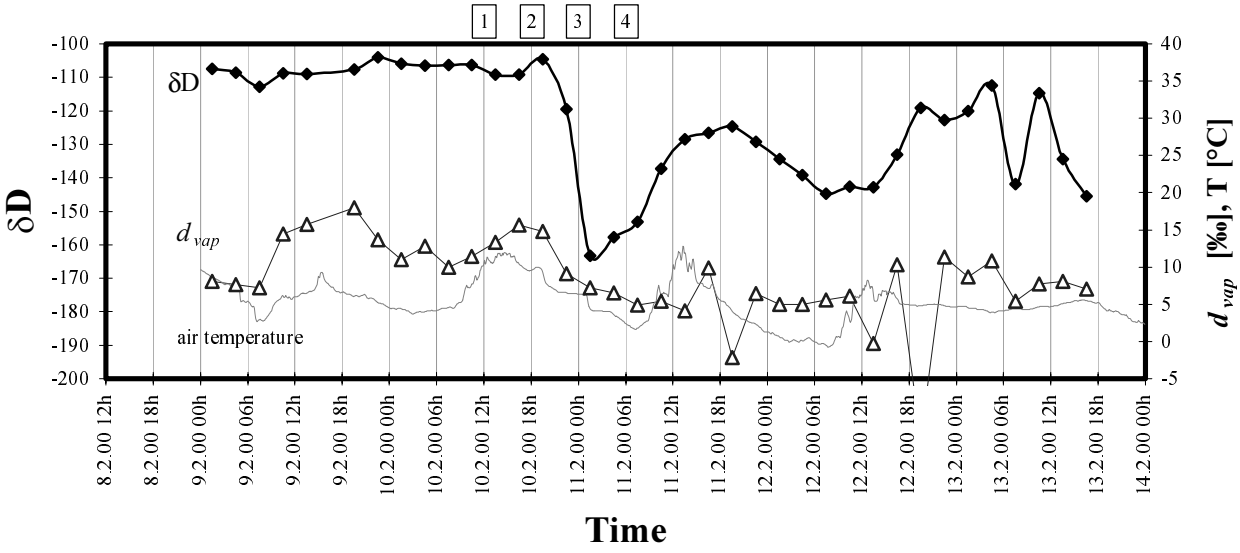

Fig 5.8 Strong short-term fluctuations of δD, d_{vap}, and air temperature over 5 days in February reflect the varying contribution of tropical and polar air masses to the mid-latitude weather conditions. The numbers on top of the diagram refer to back-trajectories illustrated in Fig. 5.9.

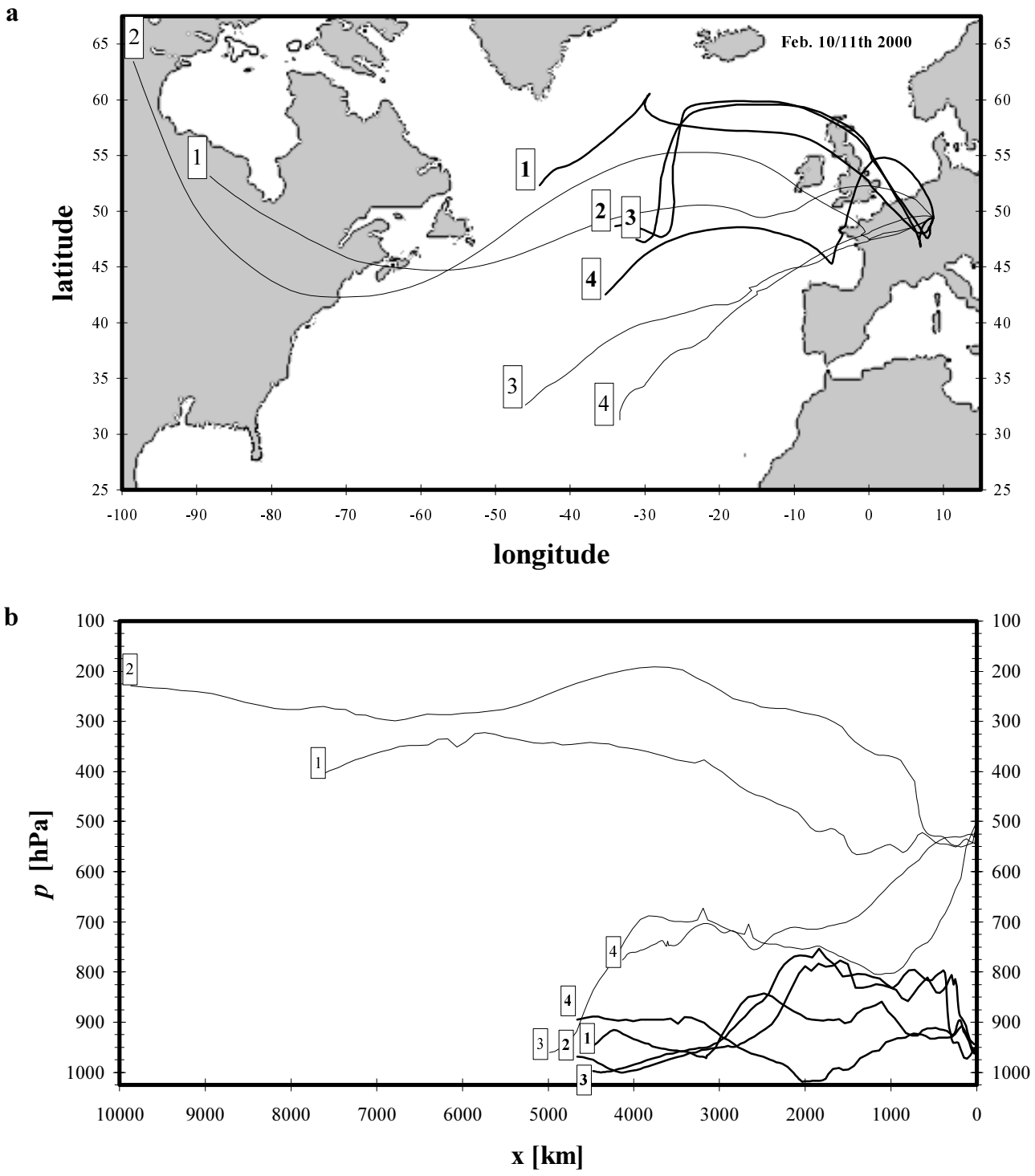

Fig. 5.9 Eight 3-D back-trajectories over 96 hours for Heidelberg at two pressure levels, bold tracks arrive at 950 hPa, thin tracks arrive at 500 hPa. The numbers 1 to 4 relate to arrival times (UTC): 1 = Feb 10th 2000 at 12h, 2 = Feb 10th 2000 at 18h, 3 = Feb 11th 2000 at 00h, and Feb 12th 2000 at 06h. (a) Plan view. (b) Cross-sectional plot along trajectory pathways: air pressure *p* versus distance from Heidelberg x.

5.4 The Isotope – Temperature Relation

In addition to the $\delta D - \delta^{18}O$ relation there also exists a highly significant spatial and temporal co-variation in isotopic composition of precipitation and mean air temperature near surface level (T) at mid- and high latitudes such that $\delta^{18}O$ (and δD) are related to T, with $\delta^{18}O$-temperature gradients ranging from 0.3 to 0.9‰ per degree Celsius (Dansgaard, 1964; Rozanski et al., 1993). The $\delta - T$ relation is primarily determined by the mean degree of rainout of the moist air mass. Monthly local air temperature is a good proxy for the mean moisture loss along the air mass trajectory because the moisture holding capacity of air is a function of temperature and the initial vapour load remains fairly constant due to little variation in the sea surface temperature.

The history of precipitation and evaporation along the air mass trajectories as well as the initial isotopic composition of vapour further influence the $\delta - T$ relation, but these parameters have little effect since they do not fluctuate very much.

Table 5.2 Calculated δ-temperature relations for arithmetic means of water vapour and weighted means of precipitation.

type of sample	**$\delta^{18}O$ [‰]**		**δD [‰]**	
water vapour Heidelberg monthly means 1981-1999	= 0.36 T – 22.4	r = 0.93	= 2.8 T – 166.9	r = 0.92
water vapour Heidelberg annual means 1981-1999	= 0.58 T – 25.1	r = 0.55	= 5.1 T – 193.9	r = 0.61
precipitation 17 GNIP stations in Central Europe monthly means 1981-1995	= 0.22 T – 10.2	r = 0.92	= 1.7 T – 75.0	r = 0.93
precipitation 17 GNIP stations in Central Europe annual means 1981-1995	= 0.59 T – 14.6	r = 0.29	= 4.5 T – 107.0	r = 0.27

The $\delta - T$ relation also holds true for water vapour, even though the $\Delta\delta/\Delta T$ gradient is stronger for water vapour than for precipitation which is due to the non-linear temperature dependence of the fractionation factors. We will discuss the temporal relation between the long-term (interannual) averages of δ and T and the short-term (seasonal) changes of δ and T. Variations of δ on time scales smaller than one month show little or no correlation with T. The reason is that the synoptic weather regime produces rapid fluctuations in the isotopic composition of water vapour without significant $\delta - T$ co-variation. Polar air masses or foehn winds, for instance, usually convey isotopically lighter moisture than air masses from sub-tropical regions even when the local surface temperature remains the same.

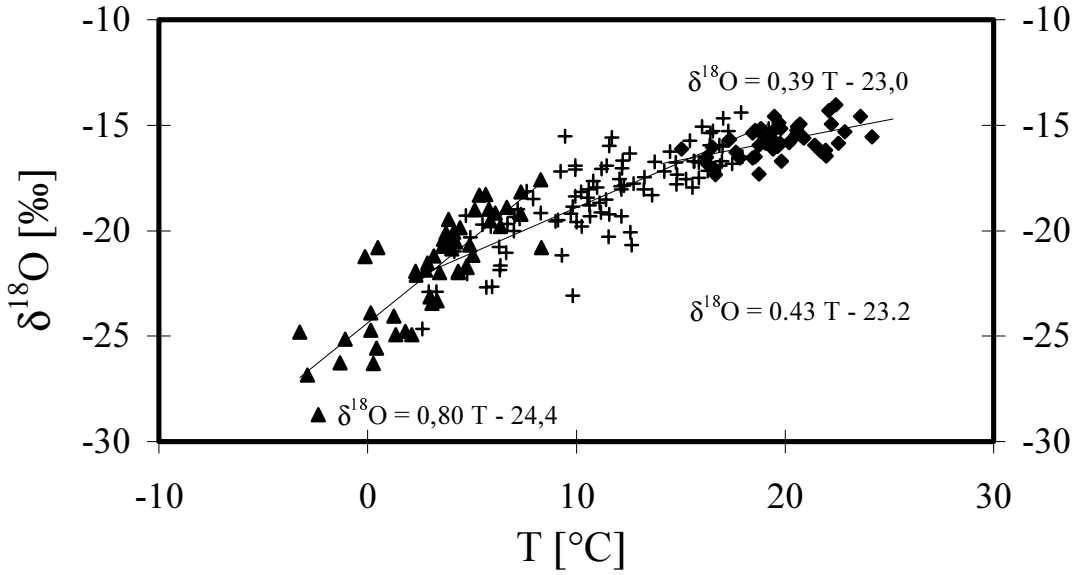

Fig. 5.10 $\delta^{18}O$ versus air temperature at ground level plot for atmospheric water vapour (monthly means from 1981 to 2000 at Heidelberg)

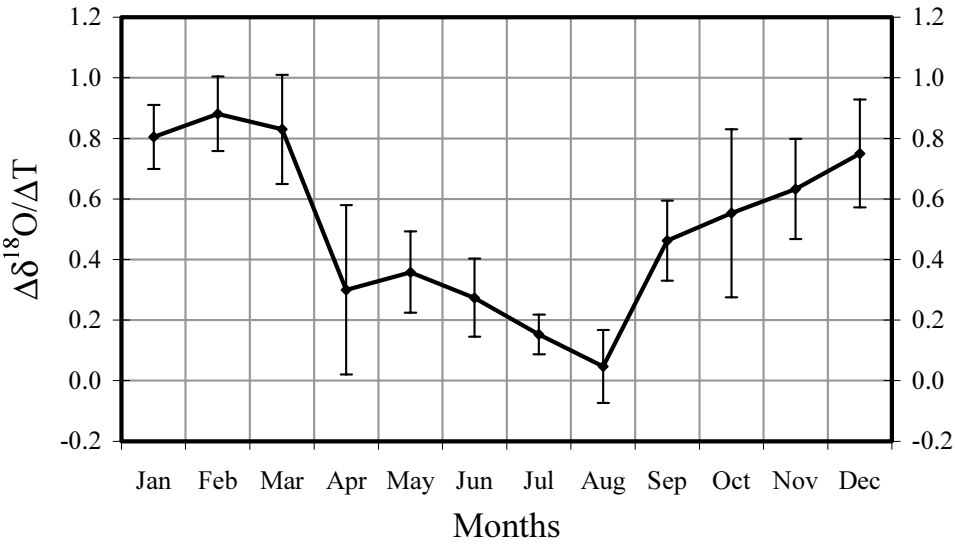

Fig. 5.11 $\Delta\delta/\Delta T$ gradients for water vapour from January to December. Summer months show the lowest $\delta - T$ gradients due to mixing with plant transpired water.

Table 5.2 gives an overview of the linear fits for annual and monthly means of the isotopic composition of atmospheric water vapour and precipitation with temperature. The linear fit was calculated to facilitate comparison of our data with other results – although Fig. 5.10 shows that the $\Delta\delta/\Delta T$ gradient decreases with increasing T. This phenomenon is well known for mid-latitude water vapour and precipitation (Jacob &

Sonntag 1991, Rozanski *et al.* 1993). Therefore, seasonal variations of $\Delta\delta/\Delta T$ gradients have been calculated by applying a linear regression fit to each month from 1981 to 2000. Fig. 5.11 shows that $\Delta\delta/\Delta T$ gradients range from 0.05‰/°C in August to 0.88‰/°C in February. Note, that correlations of single months over the years display steeper slopes than monthly means in Fig. 5.10.

The observed seasonal variations of the $\Delta\delta/\Delta T$ gradient cannot be explained by simple Rayleigh condensation, even though adiabatic cooling produces a significantly lower slope in the $\delta - T$ plot than isobaric cooling. This phenomenon is due to the decompression of air which lowers the dew-point temperature. Therefore, a larger share of moist adiabatically cooled air within one month flattens the $\delta - T$ relation. However, the share of moist-adiabatically cooled air is generally low in Heidelberg and cannot explain the discrepancy between measured values and the Rayleigh condensation model.

As has been pointed out recently by Hendricks et al. (2000), the continuous recharge of the atmosphere by evaporation must be included in simple Rayleigh models when considering $\delta - T$ relations. The breakdown of the $\delta - T$ relation at air temperatures exceeding 15°C is mainly caused by a positive sea-land temperature gradient in summer. Maritime air masses experience less condensation events over the continent in summer than in winter. Seasonal variations of the initial dew point temperature at the site of evaporation produce an 8-times lower $\delta - T$ slope than condensation and precipitation in a Rayleigh distillation process.

The variations of the relative humidity at the sampling site also affect the $\delta - T$ relation. Plotting δ-values versus dew-point temperatures instead of local surface temperatures yields a less steep slope with less curvature in the $\delta - T$ plot (Fig. 5.12).

Water vapour released by plants may be the most important reason for the flat $\delta - T$ slope in summer. Nearly 70% of continental evaporation is caused by transpiration of the vegetation. The share of water vapour recycled by evapotranspiration in any parcel of air depends critically on various parameters such as location, height above ground, vertical and horizontal mixing and the history of the air mass. The average storage of water vapour in the atmosphere over Central Europe in summer is approximately 30 mm. Regarding the mean evaporation rate over Europe of 3 mm per day in summer, this means that more than 25% of total atmospheric moisture can be attributed to evapotranspiration after 3 days of inland advection. Near the ground the share of recycled water vapour is even higher due to slow vertical mixing in the troposphere – for instance approximately twice as much as in the example shown in chapter 5.3. The water vapour released by plants has approximately the same isotope content as soil moisture, i.e. there is no isotope fractionation between soil water and transpired vapour. Soil moisture is a mix of precipitation events accumulated over the previous weeks and months. Frequent precipitation events and continuous recharge to the atmosphere by

evapotranpiration in summer leads to slight isotopic depletion of atmospheric moisture but its imprint is generally not related to surface air temperature.
The non-linear $\delta - T$ relation also explains why annual mean values display steeper slopes than monthly means. Annual temperature anomalies are usually the result of very cold or very mild winters and the isotopic depletion of water vapour in winter follows a steeper gradient than in summer.

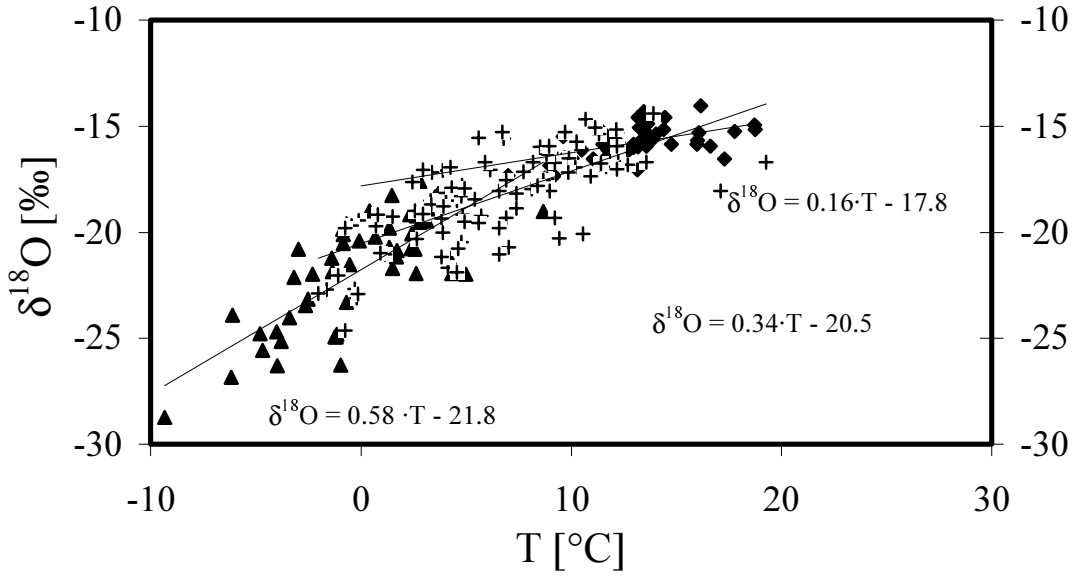

Fig. 5.12 Relation between mean monthly $\delta^{18}O$ values in water vapour at Heidelberg and mean dew-point temperatures.

6

Modelling Stable Isotopes of Water Vapour

The simulation of modern spatial and temporal stable isotope distributions in water vapour and precipitation is an important test for many paleoclimatic applications of $\delta^{18}O$ and δD in ice cores, ground water or fluid inclusions. The one-dimensional water vapour advection model described in this chapter is used to evaluate the factors that control the ^{18}O and D content of water vapour collected at Heidelberg. Variations in $\delta^{18}O$ and δD in water vapour are controlled by continuous evaporation from the surface and frequent condensation and precipitation events. The model predicted temporal variations of $\delta^{18}O$, δD and deuterium excess in water vapour at Heidelberg in good agreement with actual measurements. Only the $\Delta\delta/\Delta T$ gradient is overestimated because calculated δ values are too low in winter.

Dynamically simple Rayleigh-type condensation models are frequently applied to explain observed relationships between local air temperature and the isotopic composition of precipitation or atmospheric moisture (Craig and Gordon, 1965; Dansgaard, 1964; Jouzel and Merlivat 1984, Merlivat and Jouzel, 1979).

These models describe the isotopic composition of moisture in isolated air masses as they move away from the water vapour source and lose water through condensation and subsequent precipitation. The isotopic composition of water vapour or precipitation at a given site depends on the initial isotopic composition of the water vapour, the initial dew point temperature, the way of cooling (isobaric or adiabatic), and the final dew point temperature. Since these models have serious limitations due to the oversimplified hydrologic cycle, their predicting qualities are generally rather poor. The vapour source is often parameterized as constant in temperature, humidity and isotopic composition. Recharge to an air mass by evaporation or plant transpiration during transport is neglected. Thus, simple Rayleigh-type models cannot account for the complexity of dynamical processes in the atmosphere. Furthermore, these models cannot adjust to changes in surface topography, ocean currents, and atmospheric circulation associated with climatic changes, such as the transition from the last glacial maximum 18.000 years B.P. to the Holocene. Thus, the application of simple Rayleigh-

type models in paleoclimate studies relies on the assumption that the temporal and present-day spatial $\delta - T$ relationships are identical which may not be the case.

The implementation of water isotope cycles in atmospheric General Circulation Models (GCMs) overcomes most of the shortcomings inherent to simple Rayleigh-type models (Hoffmann *et al.* 1999, Armengaud *et al.* 1998, Jouzel *et al.* 1994, Jouzel *et al.* 1987). State-of-the-art GCMs can reproduce observed present-day temporal and spatial variations of stable isotopes in precipitation and/or water vapour fairly well. However, it should be pointed out that GCMs still lack sufficient prediction quality considering (i) seasonal variations of deuterium excess and (ii) short-term fluctuations of stable isotopes in precipitation and in water vapour. Problem (i) is important for our understanding of the hydrological cycle because deuterium excess is used to retrieve information on meteorological conditions at the vapour source from the isotopic composition of local water vapour and precipitation (Ciais *et al.* 1995, Merlivat & Jouzel 1979, Rindsberger *et al.* 1983, Petit *et al.* 1991). Problem (ii) has been addressed by Schoch-Fischer *et al.* (1984) who showed that rapid fluctuations of the isotopic composition of water vapour on time scales of one or two days are related to the actual weather regime. This work was based on a sampling network from 1981 to 1983 including Paris (France), Hanover (Germany), Cracow (Poland), and Heidelberg, providing the basis for a Rayleigh-type water vapour advection model. However, simulated isotope data were in most cases inconsistent with actual observations.

Most difficulties stem from the inability to simulate very small scale processes like convective cloud formation and rain falls on a coarse numerical grid.

This chapter presents a different approach using back trajectories to model the relationship between atmospheric transport and stable isotope composition of atmospheric moisture.

6.1 Data Description

All gridded meteorological data used as input parameters have been supplied by the Deutscher Wetterdienst (DWD). These data have been generated as meteorologic analysis fields by the Global Model (GM). The GM operates with a quasi-regular grid size of 1.125° and 19 pressure levels (Quaterly Report, DWD 1998). A first inspection of the relative humidity data frequently exhibit unrealistic values of either 0% or 100%. Dr. Kaestner from the DWD explains the bad values with an inaccurate interpolation routine within the GM and recommends to set the minimum relative humidity to 20% (personal comm. Kaestner 1999). The uncertainty of the relative humidity values > 20% is stated as ±5%. Although this domain of uncertainty seems small, section 6.2 will show that a shift of 5% in relative humidity may change deuterium excess by 5‰ or more.

The model requires either the isobaric back trajectories from the Atmospheric Environment Service (AES, Toronto, Canada) or the 3-D back trajectories calculated by the Deutscher Wetterdienst (DWD). The 3-D back trajectories are generally more precise than isobaric trajectories which are normally applied for ballone flights, only (pers. comm., Fay 1999)

6.2 Model Description

The isotopic composition of an air mass along its back trajectory is calculated in six hour time steps. The initial isotopic composition of atmospheric moisture is assumed to be in equilibrium with monthly mean precipitation over land areas. The initial maritime water vapour is assumed to be 2‰ lighter in $\delta^{18}O$ and δD than equilibrium water vapour due to kinetic fractionation accompanying evaporation (Craig & Gordon 1965). The atmospheric water vapour load variations over time and space are controlled by five processes: (1) evaporation, (2) transpiration, (3) condensation, (4) advection and (5) mixing. These processes also affect the isotopic composition of atmospheric moisture which will be discussed in the following.

6.2.1 Evaporation

Evaporation from the ocean contributes 84% of the total atmospheric moisture (Barry & Chorely 1995 p. 54). The ocean is by far the biggest source of all waters participating in the hydrological cycle. The sea surface is slightly isotopically enriched compared to the whole ocean reservoir due to superficial evaporation (Craig & Gordon 1965). The isotopic enrichment in the model is fixed to 0.5‰ for $\delta^{18}O$ and 4‰ for δD. The evaporation rate is primarily controlled by the difference between the saturation vapour pressure at the water surface and the vapour pressure of the air. High wind velocities facilitate evaporation because the wind is generally associated with the importation of fresh, unsaturated air which will take up available moisture. Over the sea the evaporation rate is generally highest in winter and lowest in summer because of higher wind speeds in the cold season and the dehydration of air over cold continents.

On the basis of Brutsaert's (1975) theory of evaporation and Merlivat & Contiac's (1975) flux equations (see chapter 4.3), a numerical evaporation model describes the dependence of the isotopic composition of atmospheric moisture on (i) the initial composition of water vapour δ_0, (ii) the local evaporation rate E, (iii) the total precipitable water W in the air column, and (iv) the isotopic composition of the evaporation flux δ_E in response to humidity, time t and other parameters:

$$\delta = \frac{E \cdot t \cdot \delta_E + W \cdot \delta_0}{E \cdot t + W} \tag{6.1}$$

W can be approximated by means of the ground-level values of air temperature T_g and relative humidity *h*: $W = h \cdot q_s(T_g) \cdot z$, where $q_s(T_g)$ denotes the absolute humidity for vapour saturation at the temperature T_g, and z = 2.5 km is the mean scale height of the absolute humidity profile. The feedback mechanism of this relationship requires a numerical solution which is shown in Fig. 6.1. The temporal evolution of deuterium excess (bold curve in Fig. 6.1) has been calculated for a continuously increasing relative humidity from 25% to 98% in response to local evaporation and a constant sea surface temperature of 15°C. The initial isotopic composition of the vapour is given by $\delta^{18}O$=
–40‰ and d_{vap} =+5‰. The evaporation rate *E* (dashed line) has been obtained from Brutsaert's (1975) model for evaporation, assuming an average wind speed of 5m/sec and a sea surface roughness of 0.05 mm (= smooth regime).

The evaporation module of the 1-D advection model is set up in the same way. Except, that *W* refers to the water vapour load of the troposphere below 700hPa.

Evaporation from lakes and rivers have not been included in the model because only 2% of continental European evaporation can be attributed to evaporation from open surface waters.

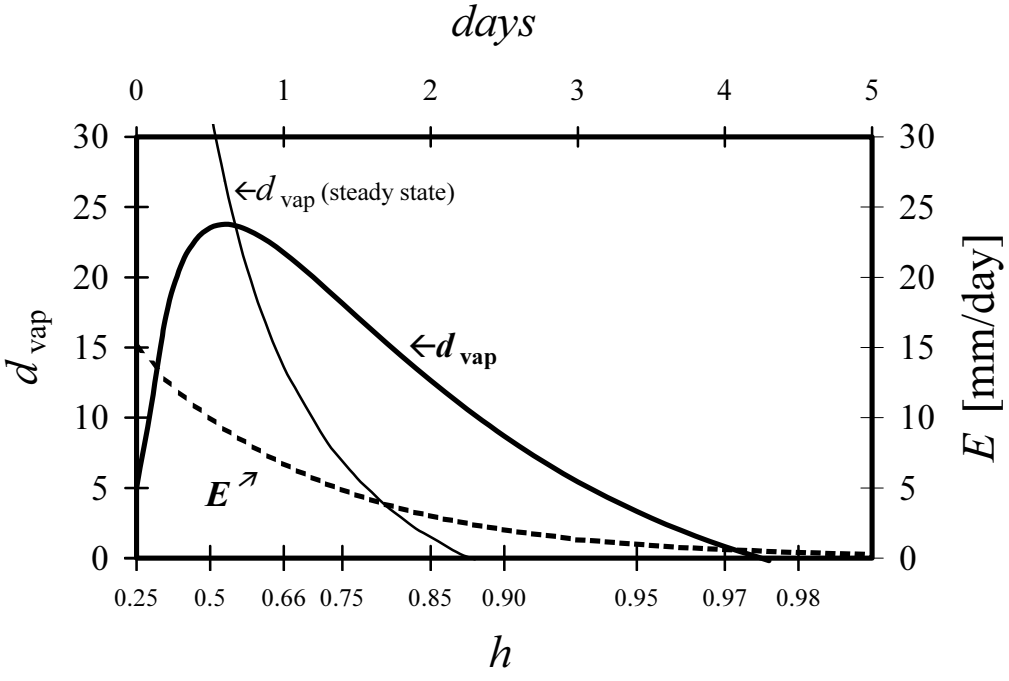

Fig. 6.1. Calculated temporal evolution of d_{vap} in an isolated air mass advected over a sea surface with constant sea surface and air ground temperature of 15°C (bold curve). The evaporation process starts with an initial humidity of 25% and d_{vap} = 5‰. The dotted curve represents the local evaporation rate *E* as a function of humidity *h*. The thin curve shows d_{vap} at steady state for a given relative humidity (independent of time).

6.2.2 Transpiration

Transpiration stands for the loss of water through the stomata in leaves. Although there is a marked evaporative enrichment of heavy isotopes in leaf water, transpiration by plants is thought to bring soil moisture without isotopic fractionation to the atmosphere (Craig & Gordon 1965, Bariac *et al.* 1994a + 1994b,Wang & Yakir 1995). Nearly 70% of central European evaporation is caused by transpiration of plants. Soil moisture is a mix of precipitation events accumulated over the last weeks and months. At mid-latitudes, transpiration during summer is generally higher than evaporation over the sea. Regarding the difficulties in distinguishing transpiration from evaporation of water from plant and soil surfaces, the combined term evapotranspiration is frequently used. Summer evapotranspiration generally exceeds precipitation in central Europe and amounts to 90 to 120 mm in July.

However, a separated treatment of evaporation from soils and transpiration by plants may be important because evaporation from soils involves kinetic fractionation (Zimmerman *et al.* 1966). Actual data from the Deutscher Wetterdienst suggest that continental vapour sources other than plant transpiration and evaporation of inteception water are small. In the model, the isotopic composition of 85% of the evapotranspiration flux is equal to unfractionated local precipitation water of the last three months – representing the isotopic composition of water released by vegetation, interception reservoir and anthropogenic sources. The isotopic composition of the remaining 15% is affected by various evaporation processes (soil evaporation, re-evaporation of rain drops and evaporation from rivers and lakes) which have been reduced to a single evaporation process and have been modeled as the evaporative flux over an open water body at ambient humidity consisting of precipitation accumulated over the last three months. Monthly isotope values for precipitation have been obtained by interpolation of stationary data from the IAEA GNIP-survey.

Table 6.1 Annual precipitation and evapotranspiration rates for Germany from the DWD

Precipitation	**[mm]**	**Evapotranspiration**	**[mm]**
soil & interception	463	vegetation	328
ground water	194	interception	72
surface runoff	122	soil	42
		re-evaporated rain	17
		surface water	11
		anthropogenic sources	11
total:	**779**	**total:**	**481**

6.2.3 Condensation

Condensation is the prerequisite of all forms of precipitation. It is generally associated with a drop in air temperature which can be the result of contact cooling, mixing of air masses of different temperatures, or cooling by adiabatic expansion of air.

Condensation to either ice or liquid water is always described as an equilibrium process. While in-cloud condensation and evaporation can be considered as closed system process, precipitation is treated as instantaneous removal from an open system. This open system process is treated as Rayleigh-type destillation. The model has no means to estimate the isotopic exchange taking place between the vapour and the liquid remaining in the cloud or drops and droplets between cloud base and ground. The effect on the vapour phase, however, is small because the fraction of liquid water in the air is generally much smaller than the fraction of vapour.

Jouzel & Merlivat (1984) propose that non-equilibrium condensation becomes important when sublimation on ice crystals takes place at temperatures below –20°C. The kinetic isotope fractionation depends on the degree of supersaturation S_i of water vapour over ice. The latter term has never been measured directly in an isotope experiment and is therefore allowed to vary as an arbitrary function of temperature in order to yield a good fit between observation and theory[7]. The treatment of non-equilibrium condensation in the 1-D advection model is difficult due to the unpredictable behaviour of S_i. Fortunately, condensation temperatures below –20°C rarely occur within the scope of the trajectories.

6.2.4 Advection

Moisture transport in the atmosphere occurs horizontally and vertically. The net transport of moisture into an air column by advection (A) can be calculated as $A = P - E - W$, where P is precipitation, E represents evapotranspiration, W is the amount of water in the troposphere between ground and 700 hPa.

In my model, the above equation is used to estimate precipitation. Thus, any time advection and evaporation generate a higher atmospheric water vapour load than really exists, surplus moisture is removed by condensation and precipitation. In the rare case when advection and evaporation yield less water vapour than observed, missing moisture can be explained by cloud formation but could also be related to uncertainties of the back trajectories or the humidity data. A surplus of moisture may be due to a convergence of air masses.

---

[7] Jouzel & Merlivat 1984: $S_i = 0.99 - 0.0060 \cdot T$
Ciais & Jouzel 1995: $S_i = 1.02 - 0.0038 \cdot T$
Hoffmann et al. 1999: $S_i = 1.00 - 0.0030 \cdot T$

6.2.5 Mixing

Modelling the mixing of different air masses requires knowledge of the vertical and horizontal distribution of stable isotopes in atmospheric moisture.

Experimental data on the vertical distribution of water isotopes have been reported by Taylor (1968, 1984), Ehhalt (1970) and He & Smith (1999). The common feature of all vertical profiles is a highly significant correlation between the isotope ratio and specific humidity in the lower and middle troposphere.

Rozanski & Sonntag (1982) showed that the steep decrease of heavy isotopes with an increasing altitude in the lower troposphere is in agreement with a Rayleigh destillation process triggered by the moist-adiabatic ascent of air and subsequent isotope exchange between water vapour, cloud water, and falling raindrops. Measurements of the isotopic composition of water vapour and cloud ice in the troposphere over the ocean (Smith 1992) showed that cloud water vapour is the primary source of atmospheric moisture in the middle troposphere, whereas lofted ice particles carried up by convective clouds release water vapour in the upper troposphere. This is a possible explanation why some vertical profiles show an increase in heavy isotopes in the upper troposphere (Ehhalt 1974).

Some vertical profiles by He & Smith (1999) and Taylor (1968) also reveal abrupt changes across the peplopause with very small isotope gradients below the peplopause. This phenomenon is the result of a well-mixed atmospheric boundary layer. The turbulent mixed layer is most pronounced in summer during daytime when surface heating acts to increase air mass instability and when free convection occurs. The isotopic composition of water vapour in the lower troposphere therefore depends on the two-way exchange between the Earth's surface and the free atmosphere.

The 1-D model does not account for air movements in vertical direction or for variations of δD and $\delta^{18}O$ at higher altitudes. The implementation of vertical mixing into the 1-D advection model was prevented by its complex nature and missing data on the thickness of the mixed layer, cloud cover and cloud water content. The model averages the vertical distribution of stable isotopes below 700 hPa. Exchange of air moisture across the 700 hPa level is not considered.

Mixing of air masses of different origin is not treated explicitly because available trajectories do not provide these information. It is important to note this may be a major shortcoming of the 1-D advection model because cooling of an air mass by turbulent mixing with another air mass results in fractionation which cannot be expressed by the Rayleigh condensation formula.

An elegant solution of this problem can be accomplieshed by using Eriksson's (1965) modifications of the Rayleigh formula for water vapour transport by eddy diffusion (replacing $\alpha - 1$ with $\sqrt{\alpha} - 1$, see also section 4.2). Since water vapour transport in the atmosphere is never entirely by advection or by eddy diffusion, an

intermediate formula should reproduce the processes in the atmsophere most adequately. Trial and error resulted in $\alpha^{0.75} - 1$ as the best modification of the Rayleigh formula.

6.3 Model results

Monthly mean values of $\delta^{18}O$, δD, and deuterium excess in water vapour at Heidelberg can be calculated as weighted means of model results generated at 6-hour intervals. This study compares the results of a 42 months model run with the record of stable isotopes in water vapour (Fig. 6.1), introduced in chapter 5. The simulated minimum and maximum δ-values in winter and summer show temporal coincidence with observations. The simulated δ-values agree fairly well with an average deviation of ±1.7‰, only. But the calculated seasonality is too strong. Obviously some δ-values in winter are too low. It is very likely that the process of continental condensation and precipitation is not well represented in the model. Very low δ-values rarely occur over the oceans where continuous evaporation smoothes out extrema in the isotopic composition of water vapour. Low δ-values in winter correspond to low specific humidity which is largely controlled by air temperature. Due to temperature inversion over the continent in winter, cloud temperatures and, in turn, dew points are likely to be underestimated in the model. This results in a higher degree of rainout and a greater isotopic depletion of water vapour in the model.

The low δ-values in winter are also reflected in an overestimation of the $\Delta\delta/\Delta T$ gradient, as can be seen from Fig. 6.2. While the observed $\Delta\delta/\Delta T$ gradient in the period of the model run is 0.29‰/°C, the model produces 0.51‰/°C. A much better agreement between simulated $\Delta\delta/\Delta T$ gradient and observation is achieved for $\delta^{18}O$-values greater than -20‰. Here, model results give 0.31‰/°C. The overestimation of the $\Delta\delta/\Delta T$ gradient – especially at temperatures below 15°C – is also inherent to GCMs fitted with isotope diagnostics (Hoffmann et al. 1999, Jouzel et al. 1991).

Some d_{vap}-values also deviate from measurements, although the seasonal cycle of d_{vap} is well represented. The monthly mean deviation in d_{vap} is ±2.3‰ – regarding the overall uncertainty of the measured d_{vap}-values (±3.1‰) the model behaviour is indeed satisfactory.

The few deviations between model and observation may be due to missing days in the isotope record (also displayed in Fig. 6.1) and the fact that the model cannot account for vertical H_2O transport. These short-comings also explain why this model cannot be applied to short-term variations of δD and $\delta^{18}O$.

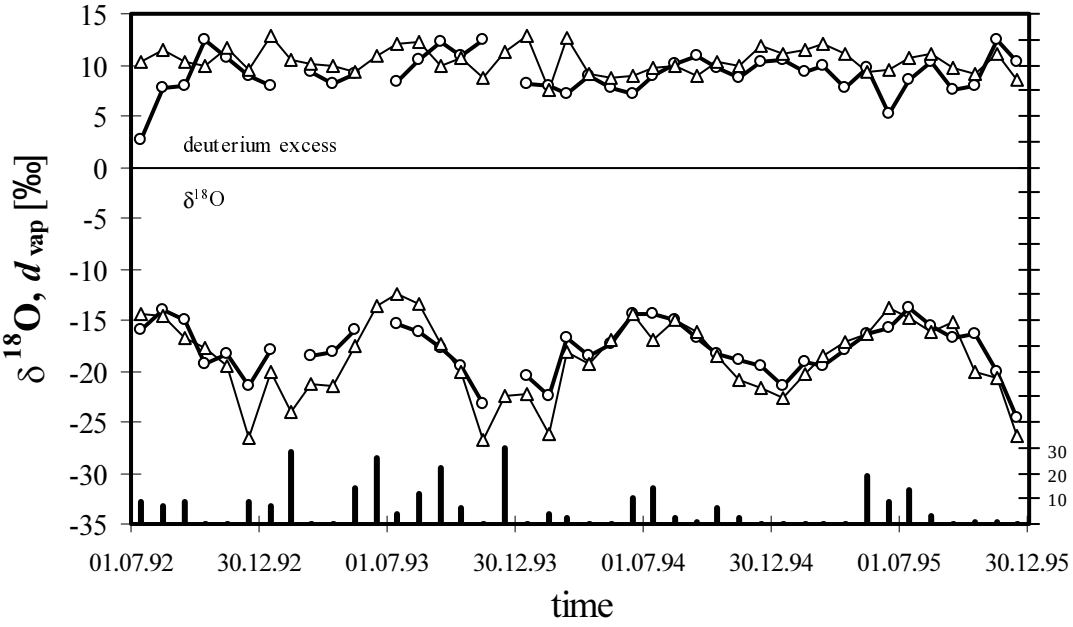

Fig. 6.1. Model results (triangles) and measured values (discs) of $\delta^{18}O$ and d_{vap} for Heidelberg over 42 months. The number of days without measurements within one months is plotted as column chart at the bottom line.

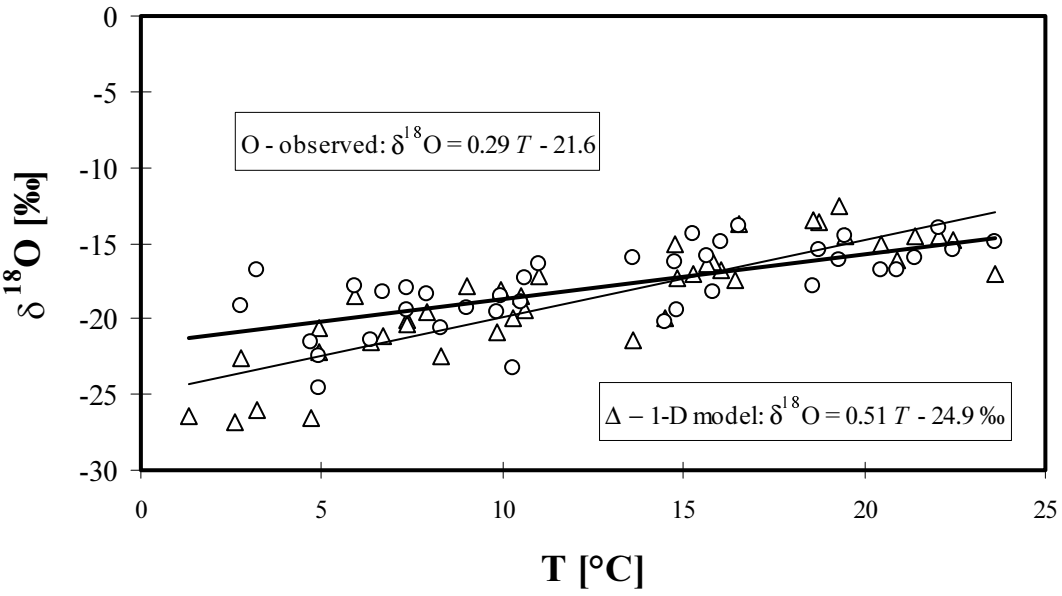

Fig. 6.2. Model calculations and observed values for $\delta^{18}O$ of water vapour at Heidelberg for the period from Jul '92 to Dec '95 as a function of air temperature. Same symbols as in Fig. 6.1.

Apart from these deficits, trajectory models may still be used to assess variations of local deuterium excess in water vapour and precipitation over time. This is of particular interest for paleoclimatic studies. The application of the 1-D advection model to the last glacial maximum requires good knowledge of regional wind fields which could be derived from GCMs (General Circulation Models). When reasonable estimates of ancient water vapour sources and past atmospheric circulation patterns are made, deuterium excess of water vapour and precipitation could be calculated and compared with values found in fluid inclusions of cave deposits or in paleo-ground waters. This could be an valuable test of our understanding of the hydrologic cycle during the last glacial maximum.

7

Conclusions

The seasonal and daily variations of $\delta^{18}O$, δD, and deuterium excess in atmospheric water vapour have been examined on the basis of a long-term record of stable isotopes in water vapour at Heidelberg. The seasonal variations show a good correlation with local air temperature and confirm earlier studies that the isotopic composition of atmospheric water vapour collected at a given site is controlled by the vapour forming process and the rainout history of the air mass. The seasonal variations are generally superimposed by strong short-term variations. To gain a better understanding of the short-term variations, $\delta^{18}O$, δD, and deuterium excess in atmospheric water vapour have been compared with the variations of the atmospheric circulation. The careful investigation of backward trajectories across Europe shows that even short passages of air masses over open water bodies may result in strong changes in deuterium excess.

For Europe, the Gulf Stream and the prevailing winds play a crucial role in establishing the δ–d phase relation because high sea surface temperatures and cold winds increase the humidity deficit in the air above sea water and, in turn, the deuterium excess in atmospheric water vapour. Continental Europe is surrounded by open water bodies that are relatively warm in October and November. This results in a high humidity deficit when cold air is advected above the Bay of Biscay and the North Sea (Fig. 5.4). This also explains why deuterium excess in Central European precipitation varies with four months time lag with respect to δ (Fig. 5.1 and Fig. 5.2).

The application of a 1-D advection model parameterized by the temperature and the relative humidity history of individual air masses can be used to reconstruct the condensation and evaporation events along 5-day backward trajectories. Although the prediction quality of the 1-D advection model for deuterium excess is not as good as for $\delta^{18}O$ and δD, the results suggest that deuterium excess in atmospheric water vapour is of regional origin.

The interrelation between deuterium excess in water vapour and advances of polar or dry continental air masses over warm surface waters has been successfully reproduced in the 1-D advection model for Heidelberg. Evaporation of regional surface

water is the most important factor to account for seasonal variations in deuterium excess. For this reason, the globally highest deuterium excess in precipitation is generally found at the lee side of continents, or in the Near and Middle East where dry continental air is advected over warm surface water. A high deuterium excess value in water vapour is generally rather short-lived. Continuous exchange with open water bodies diminishes high deuterium excess values within two days.

Studies on high-latitude precipitation often argue that distant vapour sources are responsible for the phase and amplitude of deuterium excess (e.g. Ciais et al. 1995, Johnson et al. 1989). The studies mentioned above do not deal with regional isotopic exchange between atmospheric moisture and surface water which is important to the evolution of deuterium excess in atmospheric water vapour.

The application of stable isotopes in water vapour for validating the robustness of atmospheric general circulation models has not come to a major break-through yet, mainly due to a lack of adequate records. The only study giving details on the agreement of modeled and measured isotope composition water vapour is the one of Hoffmann *et al.* (1999). Hopefully, future studies will benefit from the progress made in water vapour collection and mass-spectrometric analysis of water samples (see Chapter 3).

Many paleoclimatic archives (e.g. ice cores, fluid inclusions in speleothems, ground water etc.) preserve information about the isotopic composition of precipitation which is normally used to derive paleo-temperatures but can also be used to obtain paleo-humidities. For instance, the isotopic composition of Hungarian deep ground waters from the last cold period (14C-age = 16 ka BP) exhibit very low deuterium excess values in the range from 2 to 5‰ (Stute & Deak 1989). These values are 8 to 5‰ lower than in modern ground waters. If deuterium excess has not been modified in the course of infiltration, these values suggest there were different vapour source regions during the last cold period. Steeper meridional temperature gradients during the ice age certainly caused stronger atmospheric circulation and changed the direction of prevailing winds in response to an expanded circumpolar vortex during winter. Furthermore, a reduced share of winter precipitation (due to a extreme temperature drop in winter) preserved in ground water could also explain the low deuterium excess in ground water because summer precipitation generally has a lower deuterium excess than winter precipitation.

On the other side, cooler continents in winter also result in more efficient dehydration of the advected air, producing higher humidity deficits over the sea surface and, in turn, a higher deuterium excess in the evaporative flux. This could compensate for the effects described above and clearly shows the difficulties in interpreting deuterium excess in isotopic records.

The $\Delta\delta/\Delta T$ slope for atmospheric water vapour at Heidelberg has been shown to be lowest for the period April to August and highest from September to March. Air masses of months with mean air temperatures above 15°C show little evidence of Rayleigh-type distillation. Their $\delta - T$ relation is to a much larger extent controlled by the seasonal variations of evaporation temperatures and plant transpiration. Changes in evaporation temperatures affect the initial dew points of the air masses and flatten the $\delta - T$ slope. The $\delta - T$ slope of water vapour in equilibrium with sea water is just 0.09‰/°C.

Furthermore, the admixture of soil water to ambient moisture by plant transpiration may also flatten the $\delta - T$ slope. Trees and other plants with deep reaching roots have access to soil water which has been formed in winter from water vapour more depleted in heavy isotopes.

Similarily, the mixing of air masses by eddy diffusion lowers the $\delta - T$ slope by a factor of 2 (Erikkson 1965).

Although data on the isotopic composition of ancient precipitation preserved in geologic archives such as fluid inclusions in speleothems or ground waters provide detailed information on past climate variations, the calculation of paleo-temperatures using isotopic data in mid-latitudes is still difficult. It is likely that the $\delta - T$ gradient was steeper during the last ice age. Less transpiration by plants and lower evaporation temperatures in water vapour source regions could have established a $\delta - T$ relationship which may have resembled present-day spatial relationships in precipitation at high-latitudes.

Varying contributions of summer and winter precipitation and a possible change of the atmospheric circulation patterns in response to an expanded polar vortex adds further uncertainty to the existing problems for the calculation of paleo-temperatures from isotopic data at mid-latitudes. The correct calibration of the isotope thermometer is still a challenge for more sophisticated models which will have to pay more attention to short-term variations and the vertical dimension of the hydrologic cycle.

References

Agemar, T., Zahn, A., and Sonntag, C. (2001) An 18-years record of stable isotopes in atmospheric water vapour at Heidelberg: New implications for local deuterium excess. Tellus, submitted.

Armengaud, A.J., Koster, R.D., Jouzel, J., and Ciais, P. (1998) Deuterium excess in Greenland snow, Analysis with simple and complex models. Journal of Geophys. Research, 103(D8), 8947-8953.

Asprey, L.B. (1976) The preparation of very pure fluorine gas. Journal of Fluorine Chemistry, 7, 359-361.

Boyle, E.A. (1997) Cool tropical temperatures shift the global δ^{18}O-T relationship: An explanation for the ice core δ^{18}O-borehole thermometry conflict? Geophysical Research Letters, 24(3), 273-276.

Bariac, T., Jusserand, C., and Mariotti, A. (1990) Evolution spatio-temporelle de la composition isotopique de l'eau dans le continuum sol-plante-atmosphere. Geochim. et Cosmochim. Acta, 54, 413-424.

Barry, R.G., and Chorley, R.J. (1995) Atmosphere, Weather & Climate. Routledge, New York, N. Y.

Bechtel, C., and Zahn, A. (2001) The isotope composition of water vapour: A powerful tool to study transport and chemistry of middle atmospheric water vapor. Journal of Geophys. Res., submitted.

Brenninkmeijer, C.A.M., Kraft, P., and Mook, W.G. (1983) Oxygen isotope fractionation between CO_2 and H_2O. Isotope Geoscience, 1, 181-190.

Brenninkmeijer, C.A., and Morrison, P.D. (1987) An automated system for isotopic equilibration of CO_2 and H_2O for ^{18}O analysis of water. Chem. Geol., 66, 21-26.

Brutsaert, W. (1965) A model for evaporation as a molecular diffusion process into a turbulent atmosphere. J. Geophys. Res., 20(20), 5017-5026.

Brutsaert, W. (1975) A theory for local evaporation (or heat transfer) from rough and smooth surfaces at ground level. Water Resources Res., 11(4), 543-550.

Ciais, P., White, J.W.C., Jouzel, J., and Petit, J.R. (1995) The origin of present-day Antarctic precipitation from surface snow deuterium excess data. Journal of Geophysical Research, 100(D9), 18,917-18,927.

Craig, H. (1957) Isotopic standards for carbon and oxygen and correction factors for mass-spectrometric analysis of carbon dioxide. Geochimica et Cosmochimica Acta, 12, 133-149.

Craig, H. (1961) Isotopic variations in meteoric waters. Science, 133, 1702-1703.

Craig, H., and Gordon, L.I. (1965) Deuterium and oxygen-18 variations in the ocean and the marine atmosphere. In E. Tongiorgi, Ed. Stable Isotopes in Oceanographic Studies and Paleotemperatures, p. 9-130. Cons. Naz. Ric., Spoleto.

Cuffey, K.M., Clow, G.D., Alley, R.B., Stuiver, M., Waddington, E.D., and Saltus, R.W. (1995) Large Arctic temperature change at the Wisconsin-Holocene glacial transition. Science, 270, 455-458.

Dansgaard, W. (1954) The ^{18}O abundance in fresh water. Geochim. et Cosmochim. Acta, 6, 241-260.

Dansgaard, W. (1964) Stable isotopes in precipitation. Tellus, 16, 436-468.

DWD. (1998) Quarterly Report of the Operational NWP-Models of the Deutscher

Wetterdienst, Offenbach.

Ehhalt, D.H. (1970) Deuterium in hurricane faith 1966: Preliminary Results. Journal of Geophysical Research, 75(12), 2323-2327.

Epstein, S., and Mayeda, T. (1953) Variations of ^{18}O content of waters from natural sources. Geochimica et Cosmochimica Acta, 4, 213-224.

Eriksson, E., and Bolin, B. (1964) Oxygen-18, deuterium and tritium in natural waters and their relations to the global circulation of water. Proceedings of the Second Conference on Radioactive Fallout From Nuclear Weapon Tests, p. 675-686. Atomic Energy Commission, Germantown, Md.

Eriksson, E. (1965) Deuterium and oxygen-18 in precipitation and other natural waters - Some theoretical considerations. Tellus, 17(4), 498-512.

Faurholt, C. (1924) Studies of aqueous solution of carbonic anhydride and carbonic acid. Journal of Chem. Phys., 21, 400-453.

Gat, J.R. (1996) Oxygen and hydrogen isotopes in the hydrologic cycle. Annu. Rev. Earth Planet. Sci., 24, 225-262.

Gehre, M., Hoefling, R., Kowski, P., and Strauch, G. (1996) Sample preparation device for quantitative hydrogen isotope analysis using chromium metal. Analytical Chemistry, 68(24), 4414-4417.

Gonfiantini, R.W., Stichler, W., and Rozanski, K. (1995) Standards and intercomparison materials distributed by the International Atomic Energy Agency for stable isotope measurments. Reference and intercomparison materials for stable isotopes of light elements, Proceedings of a consultants meeting, IAEA-TECDOC-825, p. 13-29. IAEA, Vienna, 1-3 December 1993.

He, H., and Smith, R.B. (1999) Stable isotope composition of water vapor in the atmospheric boundary layer above the forests of New England. Journal of Geophysical Research, 104(D9), 11657-11673.

Hendricks, M.B., DePaolo, D.J., and Cohen, R.C. (2000) Space and time variation of $\delta^{18}O$ and δD in precipitation: Can paleotemperature be estimated from ice cores? Global Biogeochemical Cycles, 14(3), 851-861.

Hoffmann, G., Werner, G., and Heimann, M. (1999) The water isotope module of the ECHAM atmospheric general circulation mode - A study on timescales from days to several years. Journal of Geophysical Research, 103, 16871-16896.

Hoffmann, G., Jouzel, J., and Masson, V. (2000) Stable water isotopes in atmospheric general circulation models. Hydrological Processes, 14, 1385-1406.

Horita, J., and Weselowski, D. (1994) Liquid-vapour fractionation of oxygen and hydrogen isotopes of water from freezing to the critical temperature. Geochimica Cosmochimica Acta, 58, 3425-3437.

Hut, G. (1987) Consultants' Group Meeting on Stable isotope reference samples for geochemical and hydrological investigations. IAEA, Vienna.

IAEA/WMO. (1999) Global Network for Isotopes in Precipitation. The GNIP Database. URL: http://www.iaea.org/programs/ri/gnip/gnipmain.htm, Vienna.

Jacob, H., and Sonntag, C. (1991) An 8-year record of the seasonal variation of ^{2}H and ^{18}O in atmospheric water vapour and precipitation at Heidelberg, Germany. Tellus, 43B, 291-300.

Jacob, H. (1992) Deuterium und Sauerstoff-18 im Luftwasserdampf, Regen und Blattwasser. Institut für Umweltphysik, p. 42. Universität für Umweltphysik, Heidelberg.

Jakli, G., and Staschewski, D. (1977) Vapour pressure of $H_2{}^{18}O$ Ice (-50 to 0°C) and $H_2{}^{18}O$ water (0 to 170°C). Journal of the Chemical Society. Faraday Transactions, 73, 1505-1509.

Johnsen, S., Dansgaard, W., and White, J. (1989) The origin of Arctic precipitation under

present and glacial conditions. Tellus, 41B, 452-468.

Jouzel, J., and Merlivat, L. (1984) Deuterium and oxygen-18 in precipitation: Modelling of the isotopic effects during snow formation. Journal of Geophysical Research, 89(D7), 11749-11757.

Jouzel, J., Russel, G.L., Suozzo, R.J., Koster, R.D., White, J.W.C., and Broecker, W.S. (1987) Simulations of the HDO and $H_2^{18}O$ atmospheric cycles using NASA GISS general circulation model: the seasonal cycle for present-day conditions. J. Geophys. Res., 92, 14739-14760.

Jouzel, J., Koster, R.D., Suozzo, R.J., Russel, G.L., White, J.W.C., and Broecker, W.S. (1991) Simulations of the HDO and $H_2^{18}O$ atmospheric cycles using NASA GISS general circulation model: Sensitivity experiments for present-day conditions. Journal of Geophysical Research, 96(D4), 7495-7507.

Jouzel, J., Koster, R.D., Suozzo, R.J., and Russel, G.L. (1994) Stable water isotope behaviour during the last glacial maximum: A general circulation model analysis. Journal of Geophysical Research, 99(D12), 25,791-25,801.

Jouzel, J., and Koster, R.D. (1996) A reconsideration of the initial conditions used for stable water isotope models. Journal of Geophysical Research, 101(D17), 22,933-22,938.

Jouzel, J., Alley, R.B., Cuffey, K.M., Dansgaard, W., Grootes, P., Hoffmann, G., Johnsen, S.J., et al. (1997) Validity of the temperature reconstruction from water isotopes in ice cores. Journal of Geophysical Research, 102, 26471-26487.

Lippmann, J., Gröning, M., and Rozanski, K. (1999) 2nd Interlaboratory Comparison for Deuterium and Oxygen-18 Analysis of Water Sample. IAEA Report, 32.

Majoube, M. (1971) Fractionnement en oxygen-18 et en deuterium entre l'eau et sa vapeur. Journal of Chemical Physics, 10, 1423-1436.

Majoube, M. (1971) Fractionnement en ^{18}O entre la glace et la vapeur d'eau. J. Chim. Phys., 68(4), 625-636.

Merlivat, L., and Nief, G. (1967) fractionnement isotopique lors des changements d'etat solide-vapeur de l'eau à des températures inférieures à 0°C. Tellus, XIX(1), 122-127.

Merlivat, L., and Contiac, M. (1975) Study of mass transfer at the air-water interface by an isotopic method. Journal of Geophys. Res., 80, 3455-3464.

Merlivat, L. (1978) Molecular diffusivities of $H_2^{16}O$, $HD^{16}O$ and $H_2^{18}O$ in gases. Journal of Chemical Physics, 69(6), 2864-2871.

Merlivat, M., and Jouzel, J. (1979) Global climatic interpretation of the deuterium-oxygen-18 relationship for precipitation. Journal of Geophysical Research, 84, 5029-5033.

Neubert, R. (1998) Messung der stabilen Isotopomere des atmosphärischen Kohlendioxids. Institut für Umweltphysik, p. 144. University of Heidelberg, Heidelberg.

O'Neil, J.R., and Epstein, S. (1966) A method for oxygen isotope analysis of milligram quantities of water and some of its applications. Journal of Geophysical Research, 71(20), 49554961.

Oberhuber, J.M. (1988) An atlas based on `COADS' data set. Max-Planck-Instutut für Meteorologie.

Olson, M.P., Oikawa, K.K., and McAfee, A.W. (1978) A trajectory model applied to the long-range transport of air pollutants. AES-Toronto, LRTAP 78(4).

Petit, J.R., White, J.W.C., Young, N.W., Jouzel, J., and Korotkevich, Y.S. (1991) Deuterium excess in recent Antarctic Snow. Journal of Geophysical Research, 96(D3), 5113-5122.

Rindsberger, M., Magaritz, M., Carmi, I., and Gilad, D. (1983) The relation between air mass trajectories and the water isotope composition of rain in the mediterranean sea area. Geophys. Res. Letters, 10(1), 43-46.

Robert, F., Rejou-Michel, A., and Javoy, M. (1992) Oxygen isotopic homogeneity of the Earth: New evidence. Earth and Planetary Science Letters, 108, 1-9.

Roedel, W. (1994) Physik unserer Umwelt: Die Atmosphäre. Springer-Verlag, Berlin, Heidelberg.

Roether, W. (1970) Water-CO_2 exchange set-up for the routine ^{18}Oxygen assay of natural waters. International Journal of Applied Radiation and Isotopes, 21, 379-387.

Rozanski, K., and Sonntag, C. (1982) Vertical distribution of deuterium in atmospheric water vapour. Tellus, 34, 135-141.

Rozanski, K., Araguas-Araguas, L., and Gonfiantini, R. (1993) Isotopic pattern in modern global precipitation. In P.K. Swart, K.C. Lohmann, J. McKenzie, and S. Savin, Eds. Climate Change in Continental Isotopic Records, p. 1-36. American Geophysical Union.

Schoch Fischer, H., Rozanski, K., Jacob, H., Sonntag, C., Jouzel, I., Oestlund, G., and Geyh, M.A. (1984) Hydrometeorological factors controlling the time variation of D, ^{18}O, and ^{3}H in atmospheric water vapour and prcipitation in the northern westwind belt. Isotope Hydrology 1983, IAEA-SM-270/19, 3-30.

Smith, R.B. (1992) Deuterium in North Atlantic Storm Tops. Journal of the Atmospheric Sciences, 49(22), 2041-2057.

Socki, R.A., Karlsson, H.R., and Gibson, J., E. K. (1992) Extraction technique for the determination of oxygen-18 in water using preevacuated glass vials. Analytical Chemistry, 64, 829-831.

Soyez, E. (1999) Entwicklung einer neuen Sammlermethode von atmosphärischen Wasserdampf für Isotopenmessungen. Institut für Umweltphysik, p. 88. University of Heidelberg, Heidelberg.

Stewart, M.K. (1975) Stable isotope fractionation due to evaporation and isotopic exchange of falling waterdrops: Application to atmospheric processes and evaporation of lakes. Journal of Geophys. Res., 80, 1133-1146.

Stute, M., and Deak, J. (1989) Environmental isotope study (^{14}C, ^{13}C, ^{18}O, D, noble gases) on deep groundwater circulation systems in hungary with reference to paleoclimate. Radiocarbon, 31(3), 902-918.

Tanweer, A., Hut, G., and Burgman, J.O. (1988) Optimal conditions for the reduction of water to hydrogen by zinc for mass spectrometric analysis of the deuterium content. Chemical Geology, 73, 199-203.

Taylor, C.B. (1968) Die Isotopenzusammensetzung des atmosphärischen Wasserdampfs im Höhenbereich 500 bis 5000 m über Festland. Institut f. Umweltphysik, p. 54. University of Heidelberg, Heidelberg.

Taylor, C.B. (1984) Vertical distribution of deuterium in atmospheric water vapour: problems in application to assess atmospheric condensation models. Tellus, 36B, 67-72.

Thoma. (1979) Isotopenhydrologie in der ungesättigten Bodenzone: ein neues In-situ-Verfahren zur Gewinnung von Bodenfeuchteproben aus großen Tiefen, Anwendung auf der Europa-Düne bei Arachon in Frankreich, Institut für Umweltphysik. 109p. University of Heidelberg, Heidelberg.

Wang, X.F., and Yakir, D. (2000) Using stable isotopes of water in evapotranspiration studies. Hydrological Processes, 14, 1407-1421.

Yakir, D., Berry, J.A., Giles, L., and Osmond, C.B. (1994) Isotopic heterogeneity of water in transpiring leaves: identification of the component that controls the δ^{18}O of atmospheric O_2 and CO_2. Plant, Cell and Environment, 17, 73-80.

Zahn, A., Barth, V., Pfeilsticker, K., and Platt, U. (1998) Deuterium, oxygen-18, and tritium as tracers for water vapour transport in the lower stratosphere and tropopause region. Journal of Atmospheric Chemistry, 30, 25-47.